To the Graduate Council:

I am submitting herewith a thesis written by Thomas Holecek entitled "Study of Convective Flow Within a 3D Ampule Using Numerical Simulation." I have examined the final copy of this thesis for form and content and recommend that it be accepted in partial fulfillment of the requirements for the degree of Master of Science, with a major in Engineering Science.

Basil N. Antar

Dr. Basil Antar, Major Professor

We have read this thesis
and recommend its acceptance:

John G. Hopkins

Dr. John Hopkins

Ahmad Vakili

Dr. Ahmad Vakili

Accepted for the Council:

C. W. Minkel

Associate Vice Chancellor
and Dean of The Graduate School

Study of Convective Flow Within a 3D Ampule Using Numerical Simulation

A Thesis

Presented for the

Master of Science

Degree

The University of Tennessee, Knoxville

Thomas Holecek

May 1999

Dedication

To my parents,

Allen and Doris Holecek

Acknowledgements

I want to first thank my advisor, Dr. Basil Antar for his guidance, patience, and inspiring classes. I also have many thanks for Dr. Ahmad Vakili and Dr. John Hopkins for their guidance, inspiration, and wit. I was honored to have both of you on my committee. Many thanks to Dan Maxwell, Sekhar Radhakrishnan, and Adel Omrani for your help and encouragement. I also want to thank Yuxing Sun, Fangling Xiu, and Linda Engels for your assistance in this thesis.

Abstract

To model the convective flow associated with the production of non-linear optics within various gravity regimes a finite element model, using FIDAP, was constructed. This model was used to solve the Navier-Stokes incompressible equations with the Boussinesq approximation in the body force term. The solver was run for two ampule designs, one with a rectangular geometry and the other a trapezoidal geometry. The rectangular case was heated first on the side and then on the top while the trapezoidal case was only heated on the side. All cases used the fluid and thermodynamic properties of 1,2-dichloroethane. The simulation of the heating effects of the UV laser were accomplished by applying a circular heat flux to the ampule.

The results showed that the amount of gravity and heat flux strongly affected the isotherms and velocity field. These effects, for the side heated cases, influenced a much larger region of the ampule than the top heated case. This was primarily due to the geometry of the ampule and the way in which the flow interacted with the surface area. It was further shown that lowering the gravitational acceleration reduced the amount of convection in all cases creating a conduction dominated solution.

Contents

List of Figures

List of Tables

Chapter 1

Introduction

1.1 Background

The demands of the information age require that the speed of computers and networking equipment constantly improve. This will have to peak as the basic laws of physics only allow electrons to only travel at a finite speed. Because the speed of an electron is much lower than the speed of light it seems apparent that photons are better suited to carry information. Presently there is one major roadblock to implementing this technology. Logical electronic devices use non-linear switches and amplifiers made from semiconductor material to operate. In photo-electronics there are no such devices due to the lack of an optical semiconductor-like device. There is a material known as a non-linear optic (NLO) that may change this [1]. In a linear optic light is transmitted in an ordinary way, which is to say that it is governed by the laws of geometric optics. A monochromatic beam of light with a certain wavelength passed through a linear optic would maintain that wavelength despite other effects such as splitting or reflection. That same laser beam propagating through a NLO might transform into a beam of an entirely new wavelength, such as a red wavelength laser changing to blue. These affects are due to the crystalline structure of the optical material. Mathematically, the non-linearity is in the higher order Taylor series terms and the most commonly observed effects are of second and third order[2].

This non-linearity gives rises to many applications, several of which can be used in high speed computing. One such application is optical switches. Presently the hybrid switch, one that uses both optical and electrical properties is the fastest available device. Because this device requires optical/electronic signal conversions it is slower than would be with only an optical switch. By using the third order effects found in non-linear waveguide materials, it is hoped that optical switches can be produced [3]. Another application is the optical semiconductor which would use the non-linear response to produce a logic effect in a circuit[2]. More esoteric are such applications as the use of the chaos effects associated with non-linear light transmission as a data encryption scheme[4].

While the potential uses for these devices is great the traditional crystalline, inorganic, NLO's have a serious problem. Most of these material do not hold up to the rigors of heavy use and manufacturing stresses. The crystalline optics degrade rapidly in a high temperature environment. This is most problematic in manufacturing because of the heavy reliance on soldering. Both wasted material and precision manufacturing techniques will increase the production costs[5].

Organic non-linear optics have been shown to hold up better to stress related to both manufacturing and use. This will ultimately lower production costs of the product[5]. It has also been found that the organic optics are subject to less damage from light transmission than their inorganic counterparts which means a longer service life for the components[6]. One set of NLO's is known as polydiacetlyene monomers(PDAMNA). The PDAMNA class has three advantages over other organic NLOs. First they possess a crystalline structure that has "large optical nonlinearities with fast response times." They also possess stronger second and third order responses then most of their counterparts which means they can work with lower powered light sources. Also, of great importance in manufacturing is their ability to form in thin films which is ideal for component production. The preparation of the PDAMNA, shown in figure 1.1 begins with a solution of 1-2 dichloroethane mixed with a homogeneous distribution of synthesized diacetylene monomer 6-(2-methyl-4-nitroanilino)-2,4-hexadiyn-1-01 (DAMNA). The solution is then exposed to UV

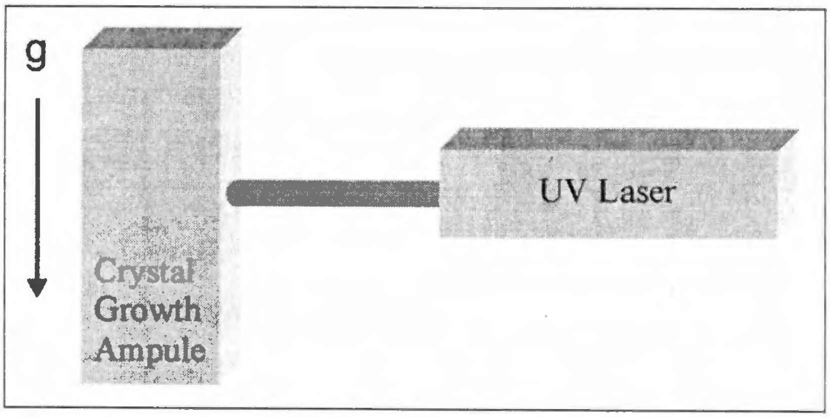

Figure 1.1: Diagram of crystal growth apparatus

radiation which produces the reaction that forms the PDAMNA chains. The process of photo-depositions occurs over the course of approximately 2 days[6].

1.2 Current Problem

The process of stimulation using the UV laser creates a serious side effect that results in a degradation of crystal quality. Because some of the UV radiation is absorbed by the solution, a convection current can form. This flow field causes imperfections in the optic as the PDAMNA film does not grow well in the region of convection[6]. Because convection currents are primarily a function of gravity it has been proposed that production in a low gravity environment might reduce convection enough to produce crystals of suitable quality. Typically a spacecraft in orbit experiences a gravitational pull on the order of $10^{-6}g_0$[7]. While this is quite small it is still enough acceleration to cause some convection. It is then necessary to develop containers that will minimize, or possibly negate, these influences. Once a container is designed it must be tested in a micro-gravity environment to insure it meets the design requirements. Because the optical manufacturing process occurs over several days it is not feasible to test the container using methods such as the drop towers or KC-135 which have a low associated cost[6]. This leaves only the Space Shuttle, the MIR space station, and eventually the International space station. All three of these platforms have extremely large associated costs, ranging into the millions of dollars, and high demand for experiment time; furthermore, in the case of MIR, an imminent shutdown. It would be a much simpler matter if a mathematical model could be built on Earth to test the container designs.

By using numerical methods to solve the governing differential equations of fluid flow a computer can be used to give an approximate solution to the flow inside the production ampule. This has two benefits, first it allows the experimenter to effectively iterate the design process as small changes can be made and tested very quickly. Secondly it may give significant cost reductions. Before the data can be used there must be some measure of the accuracy the model. To test accuracy a validation procedure must be set up.

Currently the best validation techniques are achieved by comparing the results of the computer model to the results of the experiment. But with the previously mentioned conditions even running one experimental case would be extremely expensive. Some thought will reveal that microgravity results can be yielded from 1g results. There is a dimensionless parameter, know as a Rayleigh number, that describes the character of a convective flow. The Rayleigh number is defined by

$$Ra = \frac{g\beta q'' L^4}{\alpha\nu k} \tag{1.1}$$

and g is gravitational acceleration, β is volumetric expansion coefficient, q$''$ is heat flux per unit area, L is an appropriate length scale, α is thermal diffusivity, ν is kinematic viscosity, and k is thermal conductivity. The Rayleigh number is, among other things, a function of gravity. If all the physical properties and geometry are constant then the Rayleigh number is only a function of gravity and heat flux. A microgravity result can then be be obtained on earth by holding the Rayleigh number constant and varying the heat flux. The results should be identical and thus costly space based experiments can be avoided.

It is the goal of this thesis to construct and solve a mathematical model of the various ampule configurations so that the flow and temperature field can be explored. This data will be specifically used to find the shape and vigor of the velocity field as well as the description of the temperature field. Data will be collected for several heat inputs as well as gravity magnitudes. Ultimately this will add more information to the general body of knowledge within this field as well as provide specific data to compare to future experiments.

Chapter 2

The Model

2.1 The Development of the Governing Equations

The study of almost every fluid dynamics problem begins by considering the Navier-Stokes equation. For an incompressible flow, using index notation, the equations are well known and given by

$$\frac{\partial u_i}{\partial x_i} = 0 \tag{2.1}$$

$$\rho\frac{\partial u_i}{\partial t} + \rho u_j\frac{\partial u_i}{\partial x_i} = \frac{\partial p}{\partial x_i} + \mu\left(\frac{\partial^2 u_i}{\partial x_j \partial x_j}\right) + \rho g_i \tag{2.2}$$

$$\rho c_p\left(\frac{\partial T}{\partial t} + u_j\frac{\partial T}{\partial x_i}\right) = k\left(\frac{\partial^2 T}{\partial x_j \partial x_j}\right) + \Phi + \beta T\left(\frac{\partial p}{\partial t} + \frac{\partial p}{\partial x_j}\right) \tag{2.3}$$

where u_i is the ith component of velocity, x_i is the ith direction, ρ is density, p is pressure, μ is dynamic viscosity, g_i is the ith component of gravitational acceleration, c_p is specific heat, T is temperature, and Φ is viscous dissipation function [7]. To make these equations more useful for this convection problem several assumptions, simplifications, and modifications will be made. The first assumption made is that the flow is steady state. This is valid because the production time for PDAMNA is on the order of days whereas the time necessary to reach steady state is in minutes[6]. A simplification can be made in the energy equation by ignoring the fourth term as the viscous dissipation is very small for this type of convection problem. The fifth term is also eliminated simply because incompressibility is assumed. A final simplification is to assume that the gravity vector is parallel to the vertical direction which eliminates most of the body force terms[7]. While these assumptions and simplifications help reduce the complexity of the equations it is necessary to modify the incompressible assumption to model convection.

To drive a natural convective flow fluid elements must vary in density. A warm, less dense, fluid element will rise while a cold, more dense fluid element sinks. This may lead to belief that the incompressible assumption should be ignored and the full Navier-Stokes equation solved. While this would provide a complete picture of the flow it would also be extremely tedious and require a great deal of CPU power to solve numerically. For this type of problem a better technique exists[7].

The Boussinesq approximation makes the assumption that the density of fluid varies only with temperature. It also assumes that the small variations in density only affect the body force term of the momentum equation leaving the other terms with the constant density term ρ_∞. In the body force term, the Boussinesq approximation uses the thermodynamic equation of state to modify $\rho(T)$ to become[8]

$$\rho = \rho_\infty \left[1 - \beta \left(T - T_\infty\right)\right] \tag{2.4}$$

where T_∞ is constant temperature and β is defined as

$$\beta = -\frac{1}{\rho}\left(\frac{\partial \rho}{\partial T}\right)_p \tag{2.5}$$

Once this is assumed the Navier-Stokes equations can be rewritten as

$$\frac{\partial u_i}{\partial x_i} = 0 \tag{2.6}$$

$$u_j \frac{\partial u_i}{\partial x_i} = -\frac{1}{\rho_\infty}\frac{\partial p}{\partial x_i} + \frac{\mu}{\rho_\infty}\left(\frac{\partial^2 u_i}{\partial x_j \partial x_j}\right) + \beta g_i \left(T - T_\infty\right) \tag{2.7}$$

$$\rho c_p u_j \frac{\partial T}{\partial x_i} = k\left(\frac{\partial^2 T}{\partial x_j \partial x_j}\right) \tag{2.8}$$

To obtain usable equations for the model the index notation must be expanded. This is done by associating i and j with their appropriate directional and velocity notation. For example $u_1 = u, u_2 = v, u_3 = w$ where u, v, w are the x, y, z components of the velocity, respectively. For the incompressible, steady, 3-dimensional problem, the equations of motions are

$$\frac{\partial u}{\partial x} + \frac{\partial v}{\partial y} + \frac{\partial w}{\partial z} = 0 \tag{2.9}$$

$$u\frac{\partial u}{\partial x}+v\frac{\partial u}{\partial y}+w\frac{\partial u}{\partial z}=-\frac{1}{\rho_\infty}\frac{\partial p}{\partial x}+\frac{\mu}{\rho_\infty}\left(\frac{\partial^2 u}{\partial x^2}+\frac{\partial^2 u}{\partial y^2}+\frac{\partial^2 u}{\partial z^2}\right) \tag{2.10}$$

$$u\frac{\partial v}{\partial x}+v\frac{\partial v}{\partial y}+w\frac{\partial v}{\partial z}=-\frac{1}{\rho_\infty}\frac{\partial p}{\partial y}+\frac{\mu}{\rho_\infty}\left(\frac{\partial^2 v}{\partial x^2}+\frac{\partial^2 v}{\partial y^2}+\frac{\partial^2 v}{\partial z^2}\right)+\beta g\left(T-T_\infty\right) \tag{2.11}$$

$$u\frac{\partial w}{\partial x}+v\frac{\partial w}{\partial y}+w\frac{\partial w}{\partial z}=-\frac{1}{\rho_\infty}\frac{\partial p}{\partial z}+\frac{\mu}{\rho_\infty}\left(\frac{\partial^2 w}{\partial x^2}+\frac{\partial^2 w}{\partial y^2}+\frac{\partial^2 w}{\partial z^2}\right) \tag{2.12}$$

$$u\frac{\partial T}{\partial x}+v\frac{\partial T}{\partial y}+w\frac{\partial T}{\partial z}=\alpha\left(\frac{\partial^2 T}{\partial x^2}+\frac{\partial^2 T}{\partial y^2}+\frac{\partial^2 T}{\partial z^2}\right) \tag{2.13}$$

and α is defined as the thermal diffusivity. The body force assumption sets $g_x = 0$ and $g_z = 0$ leaving only 2.11 with the body force term. This gives five equations which correspond to the five unknown variables u, v, w, p,and T.

Another important aspect of the model that must be considered is the effect of the UV laser. Two very important assumptions about the effects of the laser can be used. Since the absorptivity of quartz is extremely low, very little of the laser's energy is absorbed by the quartz so that heat generation begins at the interface between quartz and liquid. It has also been shown in previous work that the energy of the UV laser is absorbed within the first 50 μm so the laser can be approximated as surface heat flux[9]. Thus these assumptions ignore the effects of the container, save the no-slip boundary conditions at the walls

To solve this model it must have boundary conditions. For the 3-dimensional rectangular ampule there are two cases to consider: top heating and side heating. The boundary conditions for the top heating case are the following:

$$u(0.5, 0, z) = v(0.5, 0, z) = w(0.5, 0, z) = 0$$

$$u(-0.5, 0, z) = v(-0.5, 0, z) = w(-0.5, 0, z) = 0$$

$$u(0, 0.5, z) = v(0, 0.5, z) = w(0, 0.5, z) = 0$$

$$u(0, -0.5, z) = v(0, -0.5, z) = w(0, -0.5, z) = 0$$

$$u(x, y, 0) = v(x, y, 0) = w(x, y, 0) = 0$$

$$u(x, y, 4) = v(x, y, 4) = w(x, y, 4) = 0$$

$$T(-0.25 \leq x \leq 0.25, -0.25 \leq y \leq 0.25, 0) = 25^{o}C$$

x and y are bounded by

$$x^2 + y^2 \leq \sqrt{0.25}$$

$$T(-0.5 \leq x \leq -0.25, -0.5 \leq y \leq -0.25, 0) = 25^{o}C$$

$$T(0.25 \leq x \leq 0.5, 0.25 \leq y \leq 0.5, 0) = 25^{o}C$$

x and y are bounded by

$$x^2 + y^2 \geq \sqrt{0.25}$$

$$T(x, y, 4) = 25^oC$$

$$T(-0.5, 0, z) = 25^oC$$

$$T(0.5, 0, z) = 25^oC$$

$$T(0, -0.5, z) = 25^oC$$

$$T(0, 0.5, z) = 25^oC$$

$$q(-0.25 \leq x \leq 0.25, -0.25 \leq y \leq 0.25, 0) = q_0$$

x and y are bounded by

$$x^2 + y^2 \leq \sqrt{0.25}$$

$$p(x, y, z) = finite$$

The units of measure are in centimeters, temperature in centigrade, heat flux in Watt·seconds, and time in seconds. The velocity conditions come from the no-slip principle. Temperatures enforce the isothermal wall conditions except on the heating surface, which is given by q_0. Finally we assume the pressure inside the ampule is finite everywhere. We can easily show that the boundary conditions for the side heating case will be similar save adjusting the temperature and heat flux to the new location.

For the case of the Trapezoidal ampule defining the boundary conditions quantitatively will become much more difficult. It will be shown shortly that this is unnecessary as the solution method used will apply the boundary conditions in a much different way. For both cases an exact solution is presently not available so less accurate numerical means must be used. Often engineers employ numerical approximations such as Fourier series solutions or Laplace transforms but the boundary conditions chosen do not allow for use of these techniques. Presently the only available techniques of numerical approximations are numerical methods such as finite difference or finite element. For this problem the finite element method was chosen because of the availability of the tools.

For later reference it will be useful to describe this problem in a non-dimensional form. It is from this form that two important parameters can be found, the Rayleigh number and the Prandtl number. Using the dimensional equations 2.6-2.8 and the following non-dimensional variables

$$x_i^* = \frac{x_i}{L} \tag{2.14}$$

$$u_i^* = \frac{u_i L}{\alpha} \tag{2.15}$$

$$\theta^* = \frac{T - T_\infty}{\Delta T} \tag{2.16}$$

$$p^* = \frac{pL^2}{\rho \alpha \nu} \tag{2.17}$$

the non-dimensional Navier-Stokes equations are

$$\frac{\partial u_i^*}{\partial x_i^*} = 0 \tag{2.18}$$

$$\frac{1}{Pr} u_i^* \frac{\partial u_i^*}{\partial x_i^*} = \frac{\partial p^*}{\partial x_i^*} + \frac{\partial^2 u_i^*}{\partial x_i^* \partial x_i^*} + Ra\theta^* \tag{2.19}$$

$$\frac{\partial \theta^*}{\partial x_i^*} = \frac{\partial^2 \theta^*}{\partial x_i^* \partial x_i^*} \tag{2.20}$$

where the Prandtl number is defined as

$$Pr = \frac{\nu}{\alpha} \tag{2.21}$$

and the Rayleigh number as

$$Ra = \frac{\rho g \Delta T L^3}{\nu k} \tag{2.22}$$

2.2 Description of the Finite Element Method

The roots of finite element analysis began in the early 1940's with the work of Courant's 'Framework Method' (1943) but it was not until the late 1950's that the mathematical rigor of the field was standardized[10]. Until the work of Zeinkiewicz (1965) and Oden (1972) the method was primarily used by aircraft structural engineers but these new works applied the method to classes of non-linear problems such as fluid flows, heat transfer, and others[11].

The greatest advantage of the finite element method over other methods, such as finite difference, is the relative ease with which irregularly shaped domains, uncommon boundary conditions, and nonhomogeneous systems can be modeled[12]. There are improvements that can be made to the finite difference method, such as transformation functions for non-uniform geometry. Given the geometry of the current problem most numerical differential methods would work equally well. Rather than choose the method arbitrarily it must be assumed that the geometry of the ampule may evolve into a more complex form, which would favor the finite element method.

Developing a model using the finite element method is accomplished in a very methodical way. Without regard to the problem each case follows the general set of steps: discretize the domain, develop the element equations, assemble the element equations in a matrix, apply the boundary conditions, solve to convergence, post-process the results[10]. We begin by discretizing the domain.

Discretizing, or dividing up the region into smaller subdomains, is one of the most important parts of obtaining a good solution. In fact, for most engineering problems this is the most important step since virtually all of the remaining steps are highly automated. There are automated mesh tools but they still require significant engineering input to work well. When a mesh is developed one should use the expected results to guide the meshing, making sure to coarsen regions of stable, uniform flow and refining regions of complex flow. By optimizing the mesh to the geometry one can obtain good results with less computational time[10]. It is often that this is an iterative process that is only finished after some trial solutions are made. Once the mesh is constructed the element equations must be considered.

Developing the element equations is technically the most challenging part of using the finite element method. Because of this, only the general concept of the method will be discussed. Given a differential equation, the solution will be approximated into the following form

$$u \approx \sum_j u_j \psi_j + \sum_j c_j \phi_j \tag{2.23}$$

were u_j is the value of u at the jth node and ψ_j is an interpolating function, typically a polynomial. The constant coefficient c_j is used as a weighting function and ϕ_j is an approximating function. This form states that the solution to a differential equation over the jth element is found by either using an interpolating polynomial or a least squares fit[10]. One of the important benefits of finite element analysis is that a solution can be improved by increasing the number of nodes associated with an element.

Each element equation is then assembled into a matrix form. To simplify work, care is taken to insure that the resulting coefficient matrix is banded. This greatly reduces the computational time. Although the final form of the element equations is determined by the degree of the highest derivative, the general form is

$$K\overline{u} = \overline{f} \tag{2.24}$$

The K matrix is also known as the stiffness, or coefficient, matrix. This is a symmetric, banded matrix created by linear combinations of the constants associated with the interpolating polynomials or weighting functions. The vector $\overline{f}$ is created from a linear combination of boundary conditions. For a first order, steady state, differential equation the solution is simply to invert the coefficient matrix and multiply it by the $\overline{f}$ vector. For higher order equations, unsteady equations, or multiple variable equations the solution requires use of a numerical solving scheme such as Newton-Raphson, Runge Kutta, or one of many others[10].

Once a solution is obtained is is necessary to put the results into a usable form, also known as postprocessing. The only contribution from the solver is to output the results in an ordered form. Most postprocessing is done with specialized graphics package such as Tecplot, Fieldview, PV3, FIPOST, Or others. A good package will allow the user to view results in the form of charts or pictures. It may include some of its own statistical analysis software to aid interpretation.

Because of the complexity of the finite element method it is often too difficult to implement for an arbitrary problem. Because of this a market has developed for commercial packages that uses finite element analysis on problems ranging from fluids to stress analysis. There are literally dozens of packages available. Because of this availability and the need to be able to analyze multiple types of geometry it was felt that a commercial solver should be implemented to use with this problem.

Chapter 3

Solution Method

3.1 Using FIDAP to Build the Ampule Model

A flow and heat transfer finite element solving package that was available at University og Tennessee Space Institute was FIDAP. Before FIDAP was employed as the analysis package it was necessary to test that it was accurate and robust. To ensure the code was capable of giving accurate results for a wide range of parameters a simple validation case was used. Within FIDAP's documentation was an example of a natural convection case using a simple two dimensional box with flow driven by a temperature differential. The case was run and results matched both the FIDAP published results and the literature results[13, 14]. This verified that FIDAP could run natural convection in the simplest of cases. The second part of the question was to determine if FIDAP could accurately model natural convection with an applied heat flux.

A literature search was done and a case by Bejan was found [15]. A case duplicating Bejan's work was set up and run. Since this was outside of the scope of the paper the results are not mentioned except to say that the FIDAP results were in very good agreement with Bejan's results. With the confidence that FIDAP was capable of producing accurate solutions the three cases were built.

For the three cases run, as well as any other work using finite element analysis, the six steps previously mentioned in chapter 2 reduce to five steps

1. Build a CAD model of the geometry
2. Divide the region into a mesh
3. Apply the boundary conditions and physical properties
4. Run solver with appropriate options
5. Postprocess results

It is these areas that determine the solver's ease of use and for this FIDAP excels. How FIDAP addresses these five steps is by creating one, or more, separate programs to do the work. The following is a list of FIDAP's packages and their purpose:

- FIGEN: CAD and mesh generation
- FIMESH: CAD, mesh generation, and boundary conditions
- FIPREP: boundary conditions, physical properties and solver properties
- FI-BC: boundary conditions
- FISOLV: solver

- FIPOST: post-processor

- FICONV: results file format convert(post processing)

For the cases run, FIMESH was chosen to do the CAD and meshing work, FIPREP to create boundary conditions and physical properties, and both FIPOST and FICONV for post processing. FIMESH is a unique and very powerful approach to CAD and meshing, though it does not follow traditional CAD modeling techniques. The scale of a model built in a typical CAD package is linearly transformed from the scale of the real object. In FIMESH the coordinate space of the CAD model is not forced to be, and in most cases is not, linearly related to the coordinate space of the real object. Rather the model space is transformed into an integer space. While this, in itself, does not hold any advantage to the modeler it can greatly simplify the meshing. By forcing the geometry to conform to a strict set of rules it allows quick and intuitive mesh construction that can be easily refined. This type of meshing strategy does not lend itself to every geometry but for these cases it worked very well.

FIMESH also offered one other feature that made it user-friendly; its ability to easily define surfaces that would receive boundary conditions. It should be noted that the FIGEN package would have worked equally well but FIMESH offered a simpler, cleaner input file that made it easier to run in the batch mode. Whether using FIMESH or FIGEN , FIPREP was used for applying the boundary conditions and material properties.

The package FIPREP had a variety of uses. First it allowed the application of the boundary conditions to the designated surfaces. Second it was the only method within FIDAP to apply the material properties to the model. FIPREP was also used to initialize the solver with the appropriate criteria best suited for the problem. This include what type of solving scheme to use, which equations to solve for, what methods of convergence checking to use, and many other options. Since FIDAP only offers one solver, FISOLV, it will not be discussed choosing instead to describe the post processing packages.

FIDAP only comes with one post processing package, FIPOST, and it does an adequate job for very basic data collection but is very weak in most areas. One weakness of FIPOST was its inability to produce true Postscript pictures. It required a separate FORTRAN program, supplied by Fluent, to convert the FIDAP postscript to the Adobe Postscript. The conversion program, however, was not able to run in the batch mode and thus added tedium and human intervention to the process. This problem was solved by modifying the source code of the conversion program and writing a C-shell script to automate the process. While neither of these modifications were of commercial quality, they did serve to improve FIPOST usefulness to this project. Several useful analysis techniques were missing from FIPOST such as the ability to show streamlines and the lack of an integrator to show means and averages.

Because of this a package called FICONV was used. FICONV is a translator program that converts the FIDAP results file into a file type called the FIDAP neutral file. This file type was then converted to Tecplot format as UTSI holds several licenses.

Tecplot is a post processing package sold by Amtec Engineering Inc. Unfortunately Tecplot did not come the ability to read FIDAP results files or FIDAP neutral files so the author used FIPOST in conjunction with a small FORTRAN program to assemble an appropriate Tecplot file. The FIPOST input file and Fortran source code are in appendix A and B.

3.2 3-Dimensional Models

Three cases were run for the thesis work. The first two, both based on a square ampule, would be used to compare with an experiment that will be run at the Marshall Space Flight Center (MSFC) in Huntsville, AL within the next year. The two cases were identical except that one would be heated from the side and one heated from the top. A third case, using a trapezoidal ampule, was run as well. This case represented a suggested production ampule.

3.2.1 Rectangular Ampule

For the validation cases an ampule with the internal dimensions of 4.38cm x 1cm x 1cm was used. The ampule configurations are shown in figures 3.1 and 3.2. The ampule was placed so that the 4.38cm wall was parallel to the gravity vector. The heat source was applied as a circular heat flux of diameter of 0.5cm. For the top heated case the beam was placed at the center of the top surface whereas for the side case the beam was centered at a height 1.78cm from the bottom.

The mesh constructed for the square ampule cases are shown in figure 3.3 and

3.4. For the side heated case the ampule was divided in to a 47×15×11 grid. To improve the solution the elements of the heater were formed around a circle. Several iterations of this design were tested using various mesh elements such as transition regions and mixed element meshing but the improvement in the quality of the solution was negligible compared to the increased running time. When the top heating case was constructed the region was divided into a 33×17×17 grid. The top heating case had a lower element count than the side heading case. The reduction in grid density came because the flow activity was confined to an area very near the top of the ampule which meant that the majority of the mesh could be very coarse. The input file used for both cases was the same except for the change in length scales, grid densities and gravity vector.

The gravitation accelerations 980, 9.80, 0.98, and 0.0098 $\frac{cm}{s^2}$ were explored though the main focus was on 1g. The heat flux of interest was at 10, 20, and 30 mWs but results were also obtained for 1,2 and 5 mWs and several of the graphs include these results. A test matrix for this case is given in table 3.1.

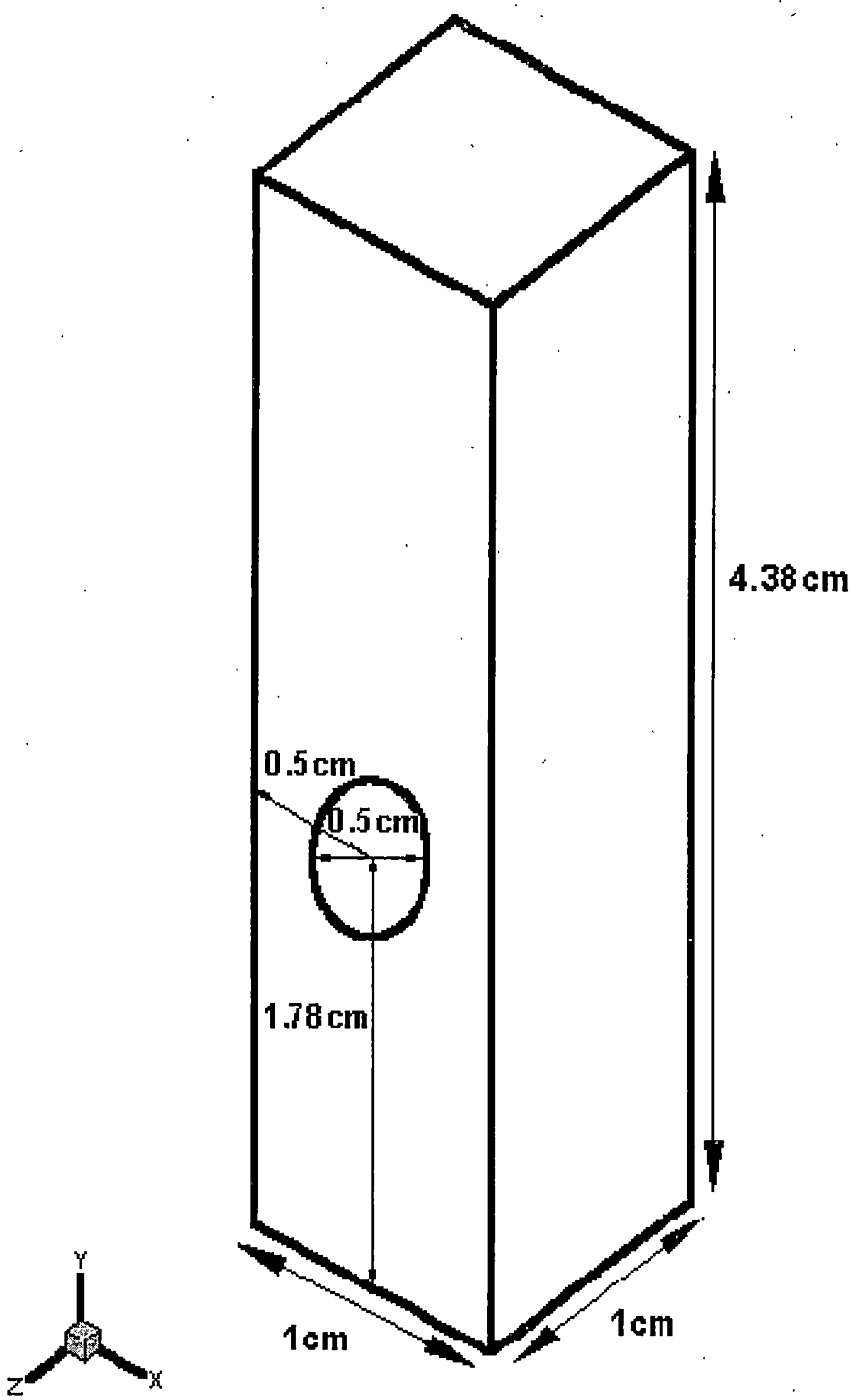

Figure 3.1: Rectangular ampule geometry with side heating

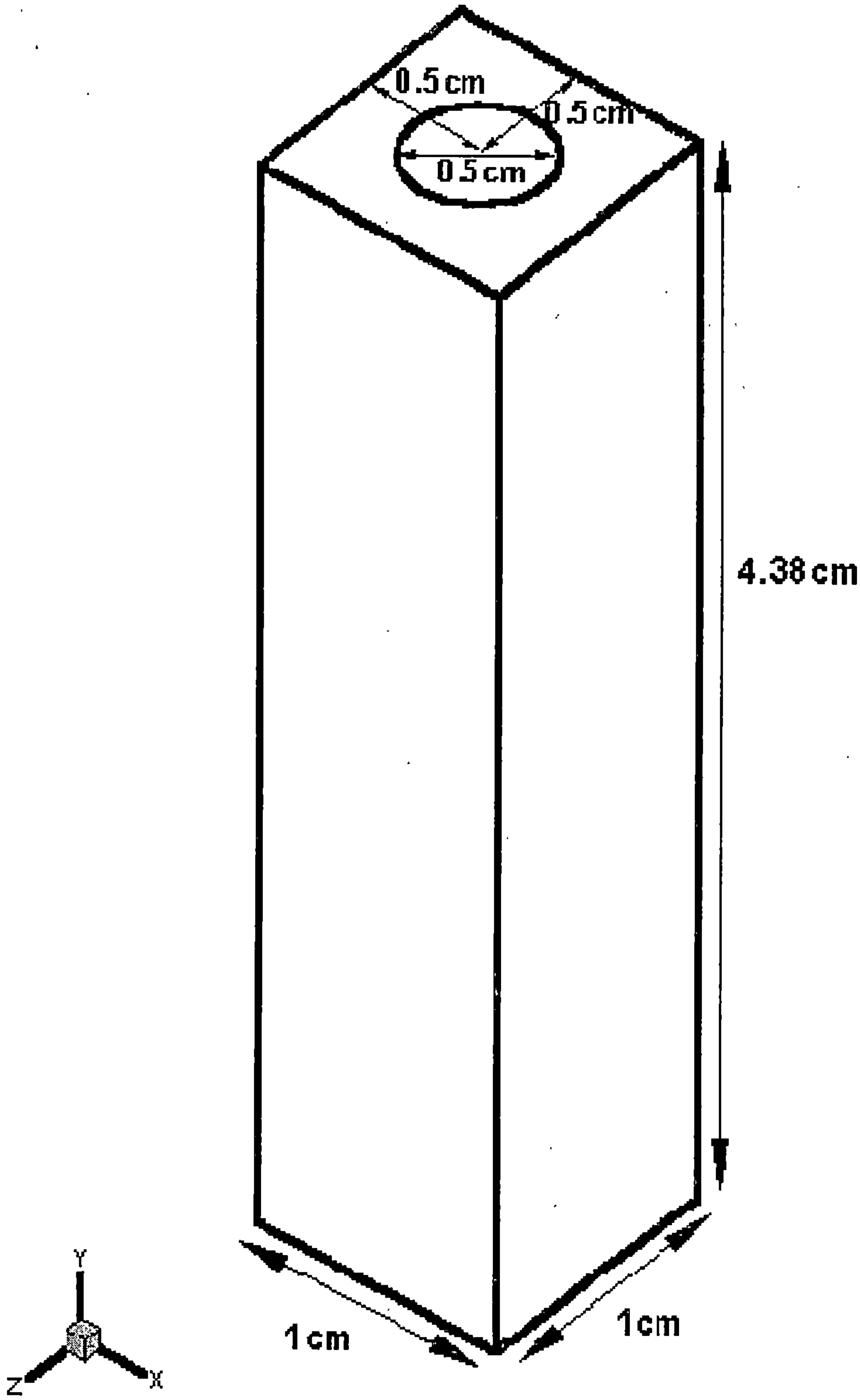

Figure 3.2: Rectangular ampule geometry with top heating

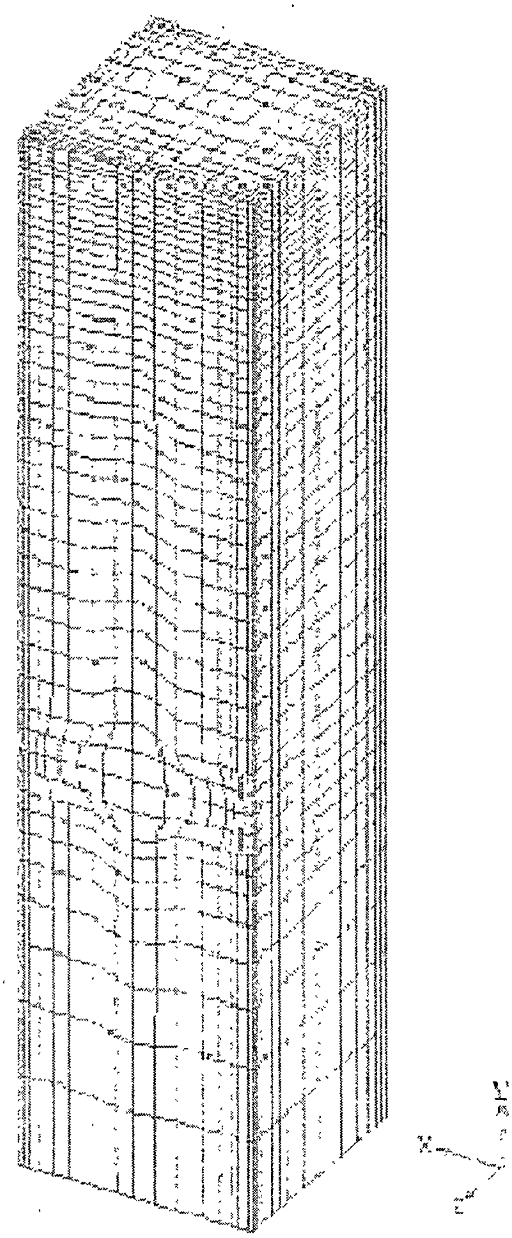

Figure 3.3: Rectangular ampule side heating mesh

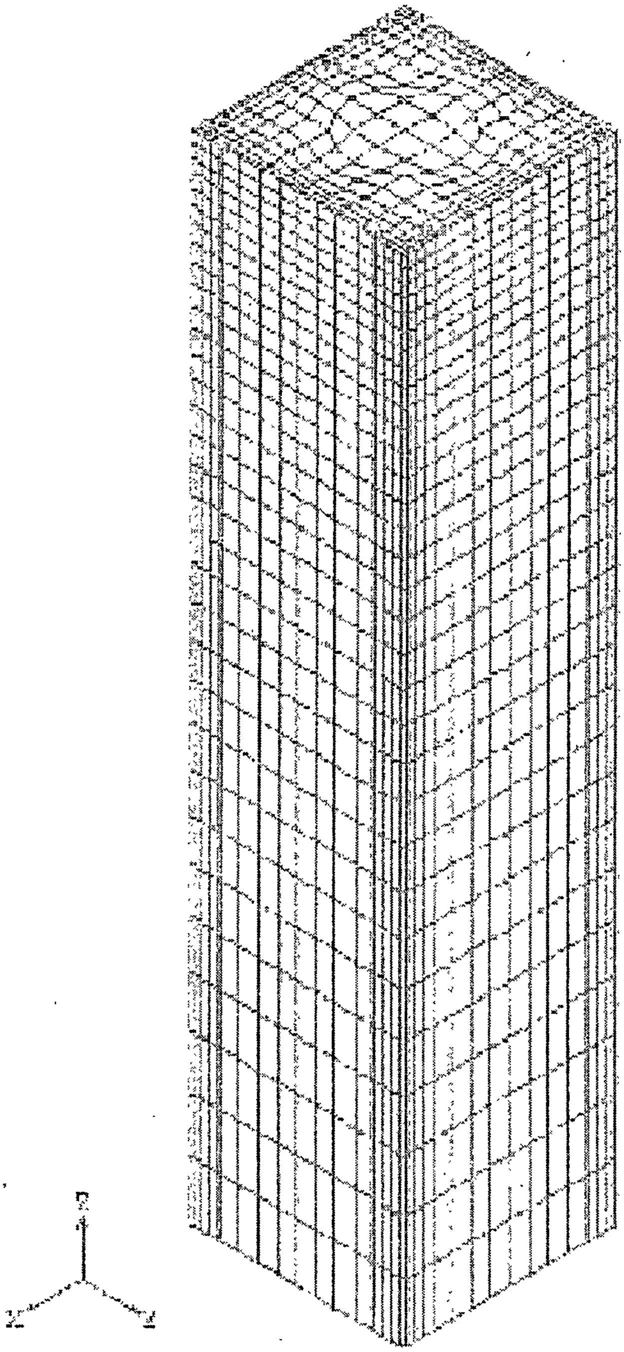

Figure 3.4: Rectangular ampule top heating mesh

Table 3.1: Ampule Test Matrix

gravity	low power(mW)	med power(mW)	high power(mW)
1g	10	20	30
10^{-2}g	10	20	30
10^{-4}g	10	20	30
10^{-6}g	10	20	30

3.2.2 Trapezoidal Ampule

A production configuration was also considered. The configuration was an ampule with the trapezoidal geometry as shown in figure 3.5. Heating took place on the side, with the spot centered horizontally and vertically on the largest wall. Side heating was the only configuration for this model. The meshing used on the trapezoidal ampule was similar to the side heated square ampule and is shown in figure 3.6. For this case a grid of $21\times29\times15$ was used. The grid distribution was similar to the side heated square ampule. This ampule used the same test matrix as shown in table 3.1

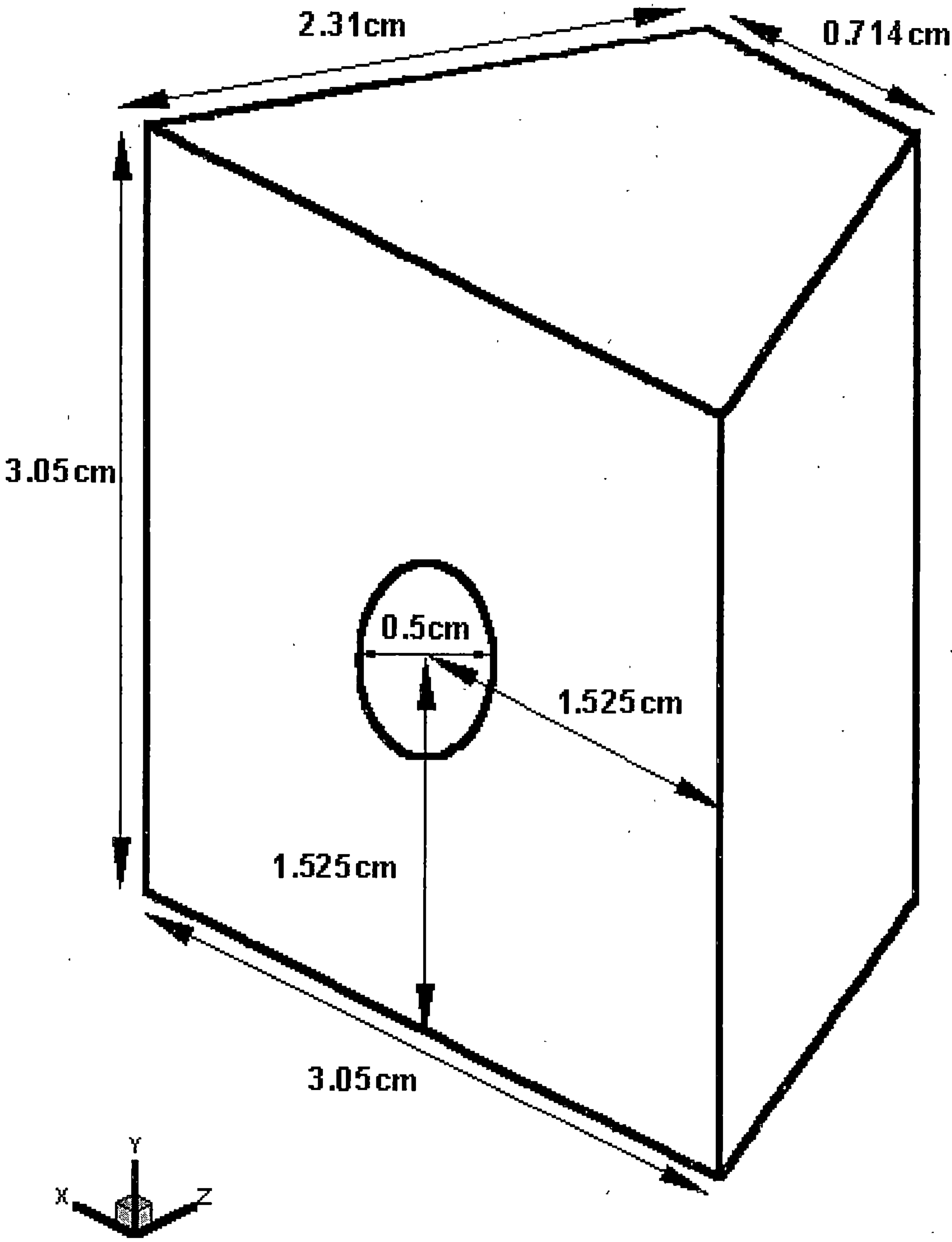

Figure 3.5: Trapezoidal ampule geometry with side heating

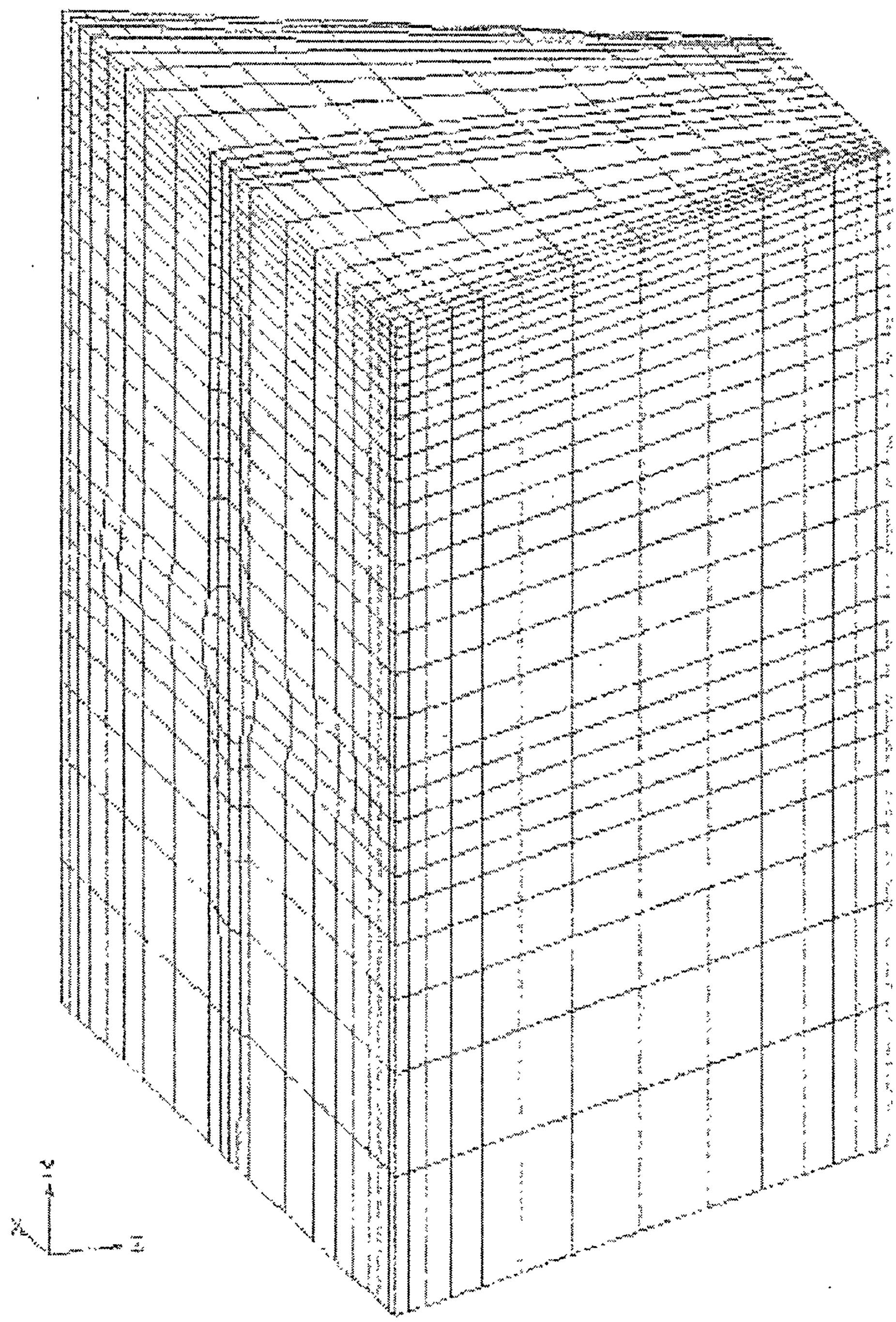

Figure 3.6: Trapezoidal ampule side heating mesh

Chapter 4

Construction of the Model

4.1 Material Properties

The working fluid was a homogeneous mixture of DAMNA and 1-2 dichloroethane. Because the ratio of DAMNA to 1-2 dichloroethane was very low the case simplified to only pure 1-2 dichloroethane[6]. The model would make use of two other assumptions about the properties of the dichloroethane substance: it would be at a room temperature of $298K$ and the properties would not vary with temperature. This assumption was verified by the results of the validation model when run with this fluid. The validation case shown only a few degrees of temperature variation.

The necessary fluid properties are from the simplification of the Navier-Stokes equations. The fluid density ρ, thermal conductivity κ, specific heat c_p, viscosity ν, and the coefficient of thermal expansion β all had to be defined. The best estimate of density came from the work of Malhotra et. al[16]. Their estimate was found to be

$$\rho = -0.86457 + 1.49656 \times \frac{10^3}{T} - 3.68056 \times \frac{10^5}{T^2} + 3.263 \times \frac{10^7}{T^3} \qquad (4.1)$$

for temperatures in the range of $278K$ to $338.15K$ where ρ is expressed in $g \cdot cm^{-3}$ and T in K. The fit curve had a rms deviation of 1.32×10^4 from the experimental data. This article was also useful in finding the viscosity. They found a relationship of temperature to viscosity of

$$\ln \nu = -3.926 + \frac{1091}{T} \qquad (4.2)$$

where the temperature was in K and ν in $MPa \cdot sec$. The range for this was from $273.15K$ to $373.15K$ and from $288K$ to $303K$ the data was within 1 percent of the experimental data. This was at a pressure $0.1MPa$[16]. The specific heat data came from a paper by Yaws and Pan who found that the relationship of specific heat and temperature was

$$c_p = 130.24 - 0.177718T + 5.385718 \times 10^{-4} T^2 \qquad (4.3)$$

where c_p has the units of $\frac{Joule}{g-mol \cdot K}$ This approximation was valid over the range of $238K$ to $387K$ [17]. The thermal conductivity came for Qun-Fang, et.al[18]. From their research they calculated the thermal conductivity of 1,2-dichloroethane to be $0.1335\frac{W}{mK}$. This is compared to the previously accepted literature value of $0.1351\frac{W}{mK}$. Based on the ability to maintain low temperature variations the uncertainty of the experiment was within 0.7 percent and for 1,2-dichloroethane the standard deviation

(σ) of the experiment was 2×10^{-4}.

The best estimate for the thermal expansion coefficient was the approximation used by Paley[6]. It was estimated to be around $1.2 \times \frac{10^{-3}}{K}$. The set of significant properties and the values are given in table 4.1.

Table 4.1: 1-2 Dichloroethane properties at 25°C.

Density	1.2436 $\frac{g}{cm^3}$
Specific Heat	0.2093 $\frac{cal}{g \cdot K}$
Conductivity	3.21E-4 $\frac{cal}{s \cdot cm \cdot K}$
Viscocity	8.15E-3 $\frac{g}{cm \cdot s}$
Volumetric Expansion	1.20E-3 $\frac{}{K}$
Kinematic Viscocity	6.55E-3 $\frac{cm^2}{s}$
Thermal Diffusivity	1.23E-3 $\frac{cm^2}{s}$

4.2 Method of Running FIDAP

FIDAP, like any numerical solver, must be used within its limitations, and buoyancy driven, convection dominated flows were within FIDAP's stated capabilities. Because the equations of motion are highly non-linear care must be used in obtaining a steady state numerical solution particularly at the moderate to high Rayleigh number flows. Numerical solvers will have difficulty at Rayleigh numbers as low at 10^4 and this is true with FIDAP. The recommended technique is to start with a small Rayleigh number, between 1 and 1000 and slowly work up to the desired range[13]. With this in mind the solution is obtained by the following method. Several runs are made with a heat flux corresponding to following definition of the Rayleigh Number

$$Ra = \frac{g\beta q'' L^4}{\alpha\nu\kappa} \tag{4.4}$$

where a characteristic length , L, was assumed to be 1cm for the rectangular ampule and 2cm for the trapezoidal ampule[15]. This definition of the Rayleigh number varies from the earlier definition in that it is derived from using heat flux boundary conditions instead of constant temperature conditions.

Using this definition heat fluxes of 10mW to 30mW put Rayleigh number into the range of 10^7. It is well know that the onset of turbulence in a enclosed convection problem occurs near this Rayleigh so a great deal of caution was taken. Three cases were run to a Rayleigh number range of 10^8 using laminar flow assumptions and then two turbulence models; $\kappa - \epsilon$ and mixing length. When each of these techniques were combined with the recommended heat flux ramping the results were in good agreement and showed a stable flow field. By exceeding the Rayleigh number range and finding stability it would be assumed that the standard Navier-Stokes equations could be used rather then the time averaged equations. The ramping techniques used in all three cases are shown in table 4.1 to 4.4.

Table 4.2: Rayleigh Number Increments and Corresponding Heat Fluxes for Rectangular Geometry

Ra	q(mW)	q" ($\frac{cal}{s \cdot cm^2}$)
10^3	1.806×10^{-6}	2.197×10^{-7}
10^4	1.806×10^{-5}	2.197×10^{-6}
10^5	1.806×10^{-4}	2.197×10^{-5}
5×10^5	9.03×10^{-4}	10.985×10^{-5}
10^6	1.806×10^{-3}	2.197×10^{-4}

Table 4.3: Heat Flux increments for Rectangular Geometry

q(mW)	q" ($\frac{cal}{s \cdot cm^2}$)
$1mWatt$	1.216×10^{-3}
$2mWatt$	2.433×10^{-3}
$5mWatt$	6.082×10^{-3}
$10mWatt$	1.216×10^{-2}
$20mWatt$	2.433×10^{-2}
$30mWatt$	3.649×10^{-2}

Table 4.4: Rayleigh Number Increments and Corresponding Heat Fluxes for Trapezoidal Geometry

Ra	q(W)	q" ($\frac{cal}{s \cdot cm^2}$)
10^3	1.467×10^{-7}	1.206×10^{-7}
10^4	1.467×10^{-6}	1.206×10^{-6}
10^5	1.467×10^{-5}	1.206×10^{-5}
5×10^5	7.335×10^{-5}	6.030×10^{-5}
10^6	1.467×10^{-4}	1.206×10^{-4}

Table 4.5: Heat Flux increments for Trapezoidal Geometry

q(W)	q" ($\frac{cal}{s \cdot cm^2}$)
$1mWatt$	1.216×10^{-3}
$2mWatt$	2.433×10^{-3}
$5mWatt$	6.082×10^{-3}
$10mWatt$	1.216×10^{-2}
$20mWatt$	2.433×10^{-2}
$30mWatt$	3.649×10^{-2}

Chapter 5

Model Results

5.1 Rectangular Ampules

The rectangular geometry of 1cm$\times$1cm$\times$4.38cm, using a 0.5cm diameter spot heater placed on the side and then the top were the first cases run. Several incremental throttling cases, starting with a Rayleigh number of 10^3, were run until the level of interest was reached; 10mW to 30mW. Within the region of interest three cases were run: 10mW, 20mW, and 30mW. For these cases the focus was on two physical properties, the temperature field and the flow field. The temperature field would provide information on where the maximum temperature occurred and how far into the fluid the isotherms extended. To simplify comparisons between cases a reference temperature of 25°C was used. This was accomplished by setting the border thermal conditions to zero. This was acceptable because of the perfect fluid assumptions. Interest in the flow field was focused on the maximum velocities of the fluid and shape of the convection cells. The velocity given is the normalized velocity, or speed, of the vector field. This was chosen as it better represented the strength of the flow.

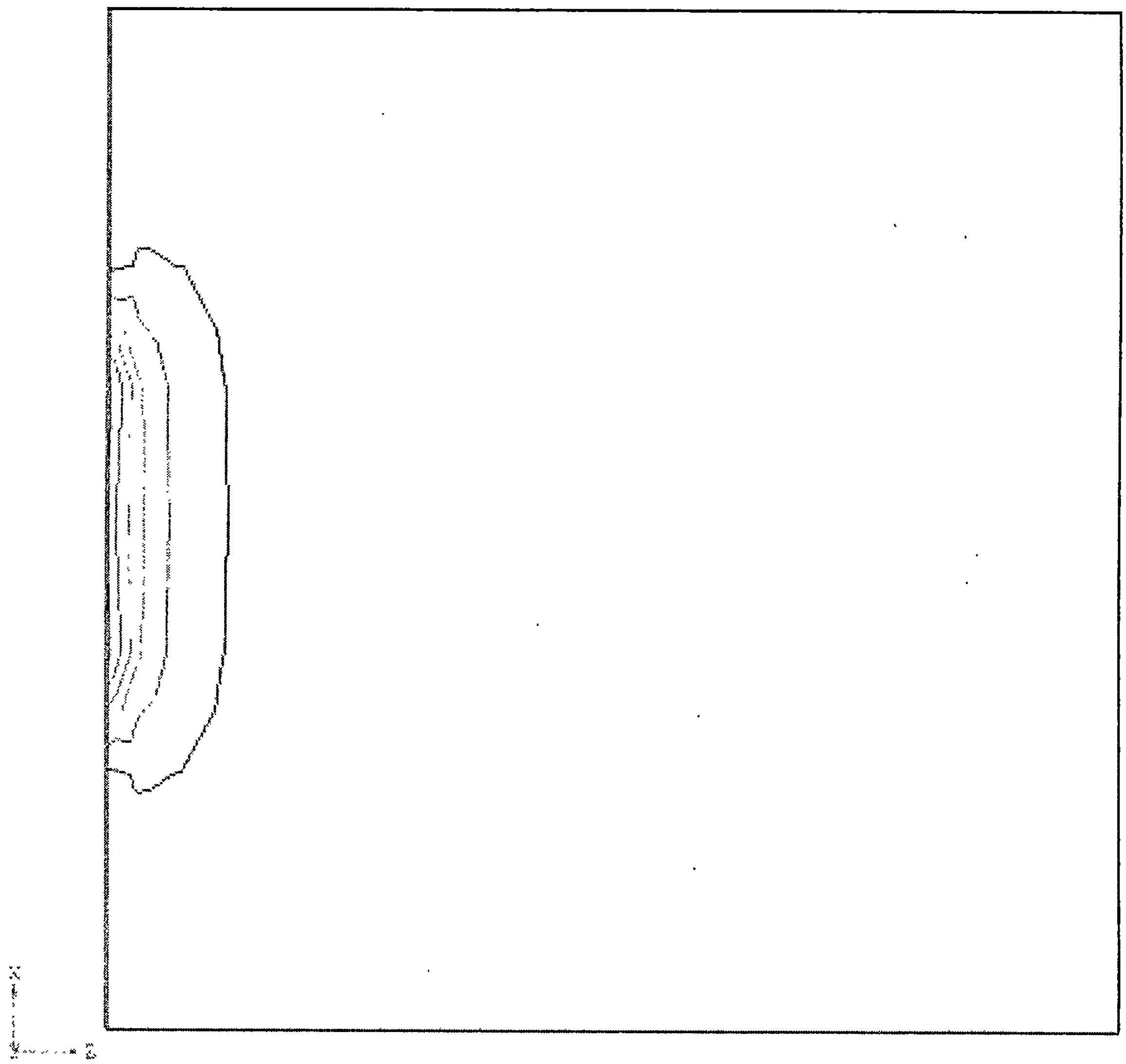

Figure 5.1: Top view of isotherms on slice at y=0cm for 10mW applied to a 0.5cm diameter spot

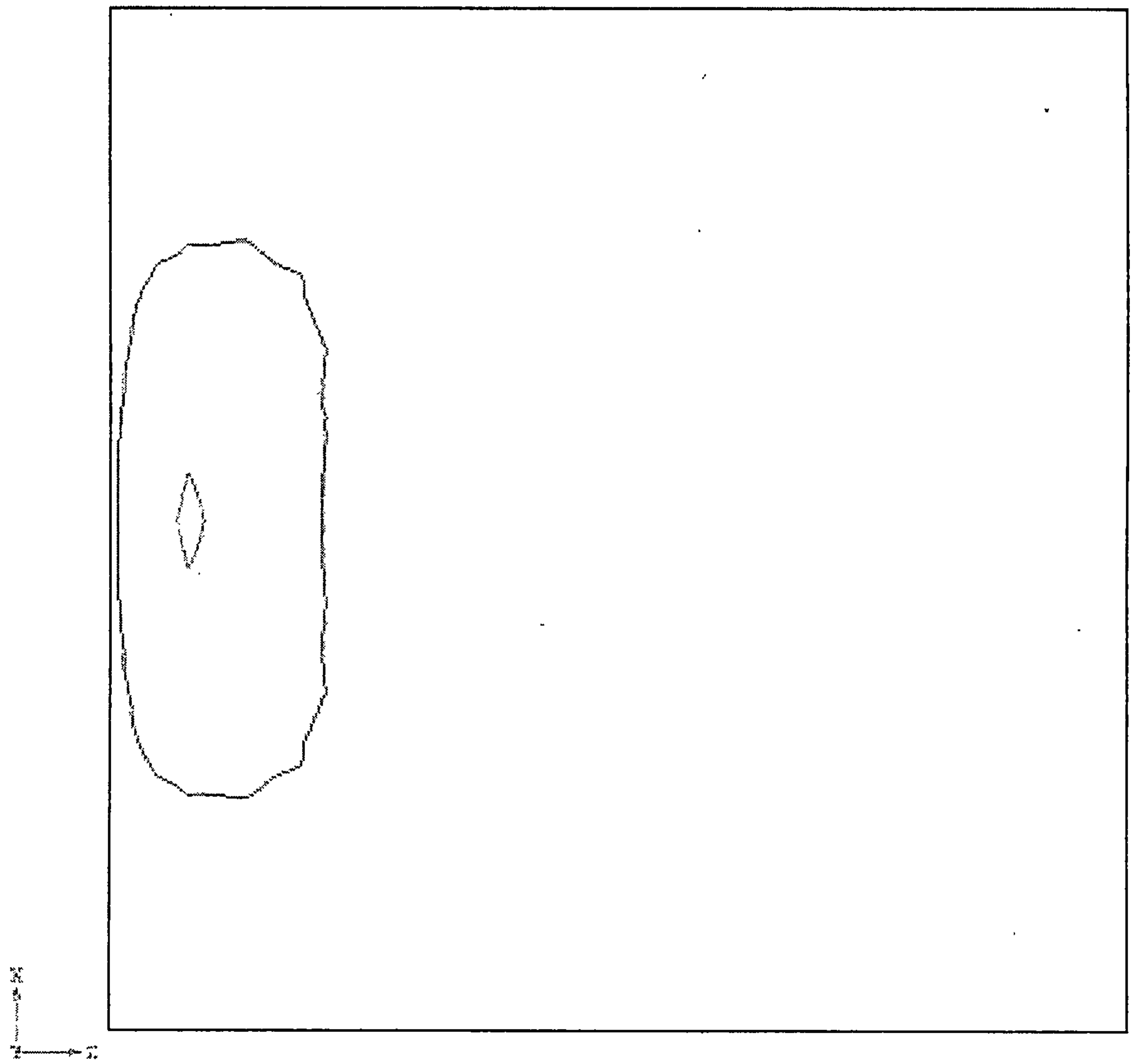

Figure 5.2: Top view of isotherms on slice at y=0.5cm for 10mW applied to a 0.5cm diameter spot

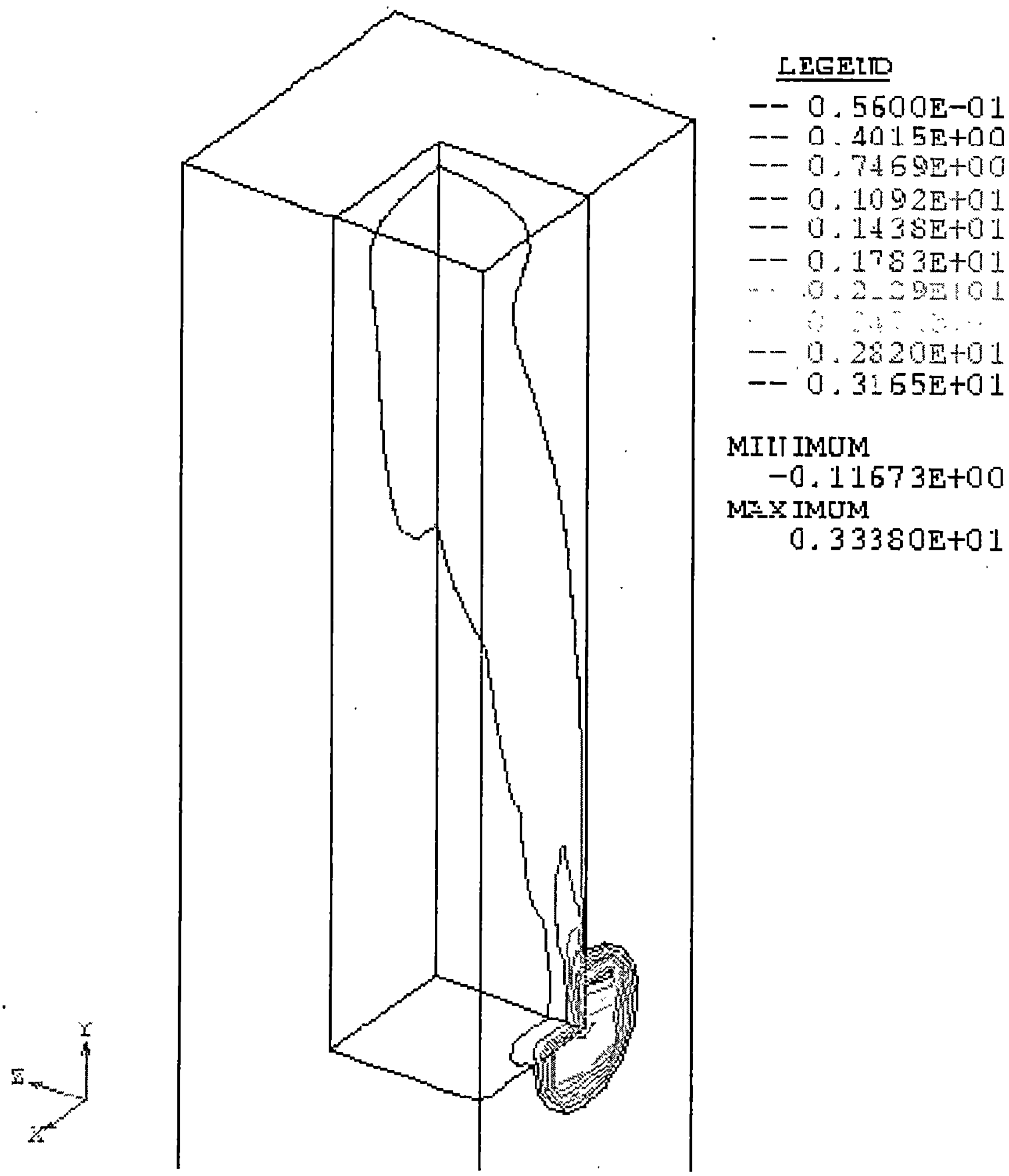

Figure 5.3: Isotherms on corner cut for 10mW applied to a 0.5cm Diameter Spot

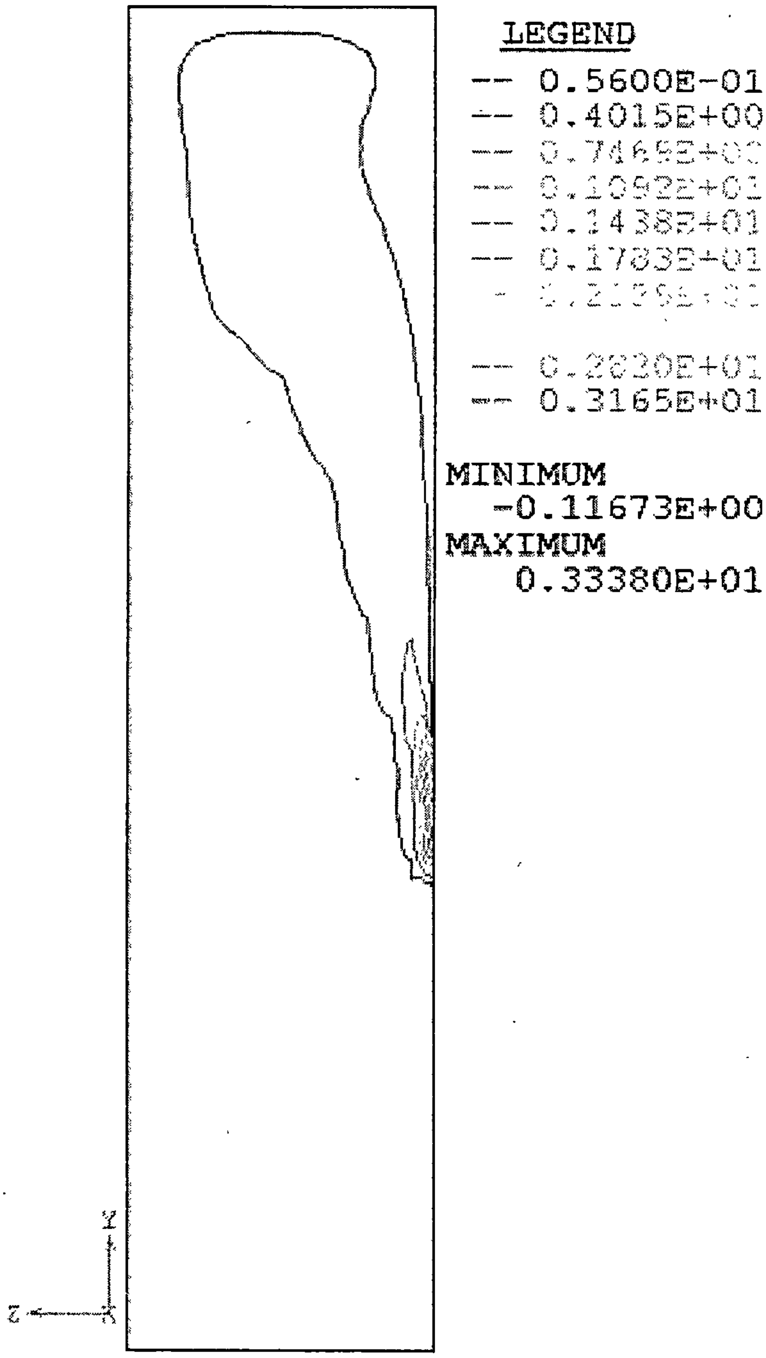

Figure 5.4: Isotherms on the symmetry plane with 10mW applied to a 0.5cm diameter spot

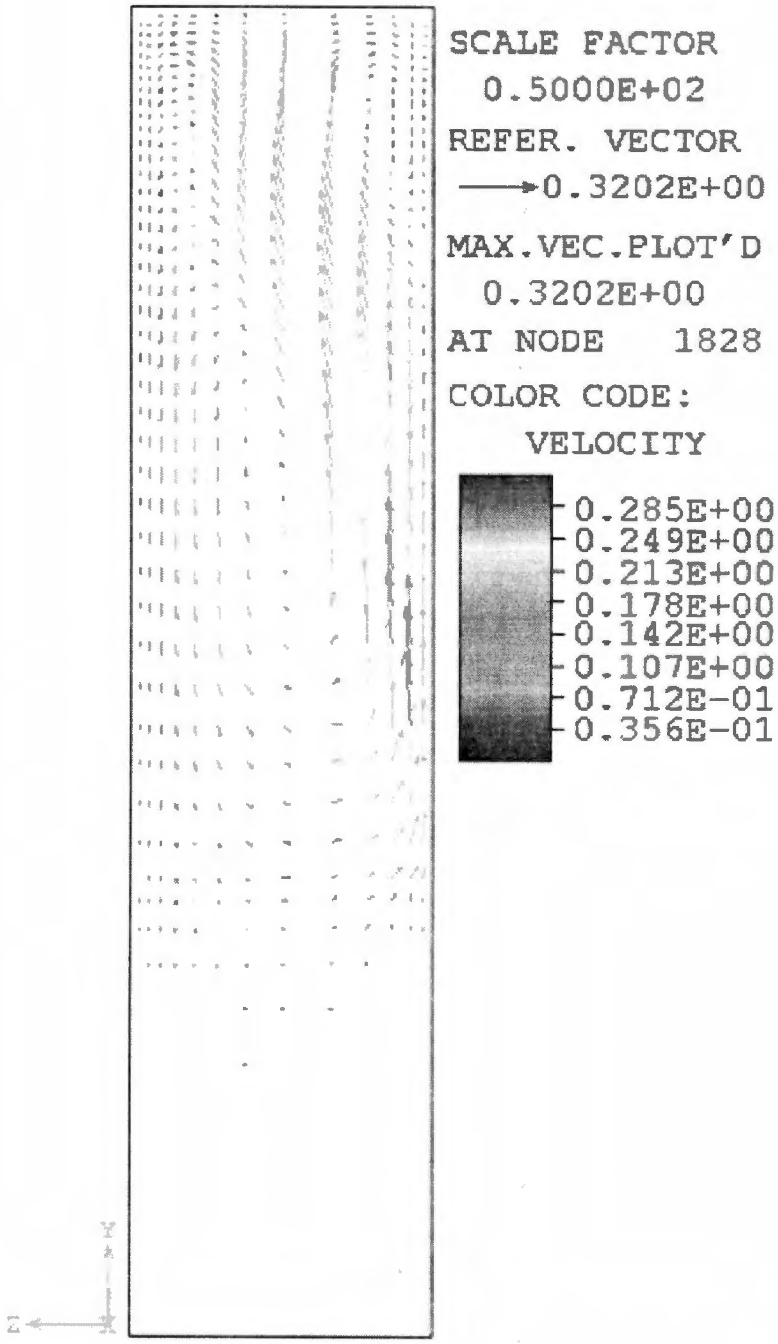

Figure 5.5: Velocity vectors on the symmetry plane with 10mW applied to a 0.5cm diameter spot

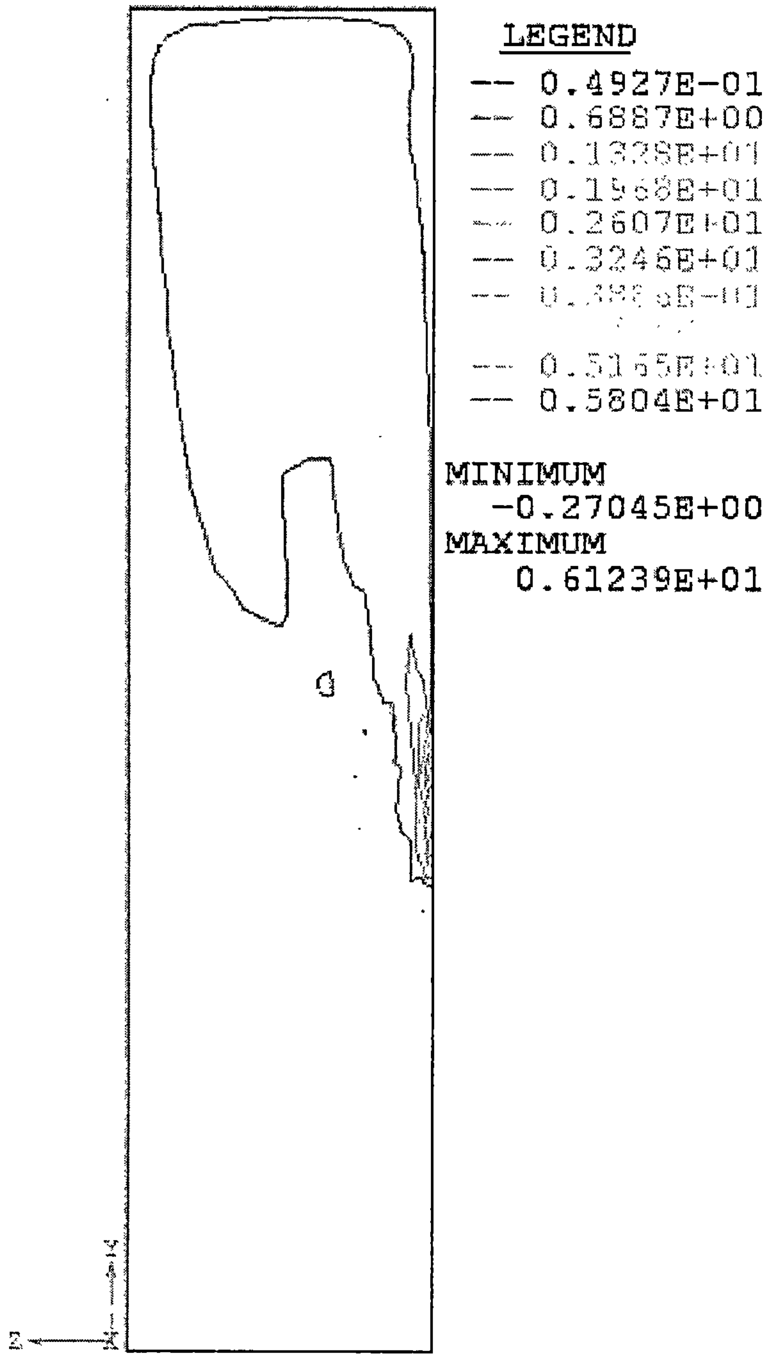

Figure 5.6: Isotherms on the symmetry plane with 20mW applied to a 0.5cm diameter spot

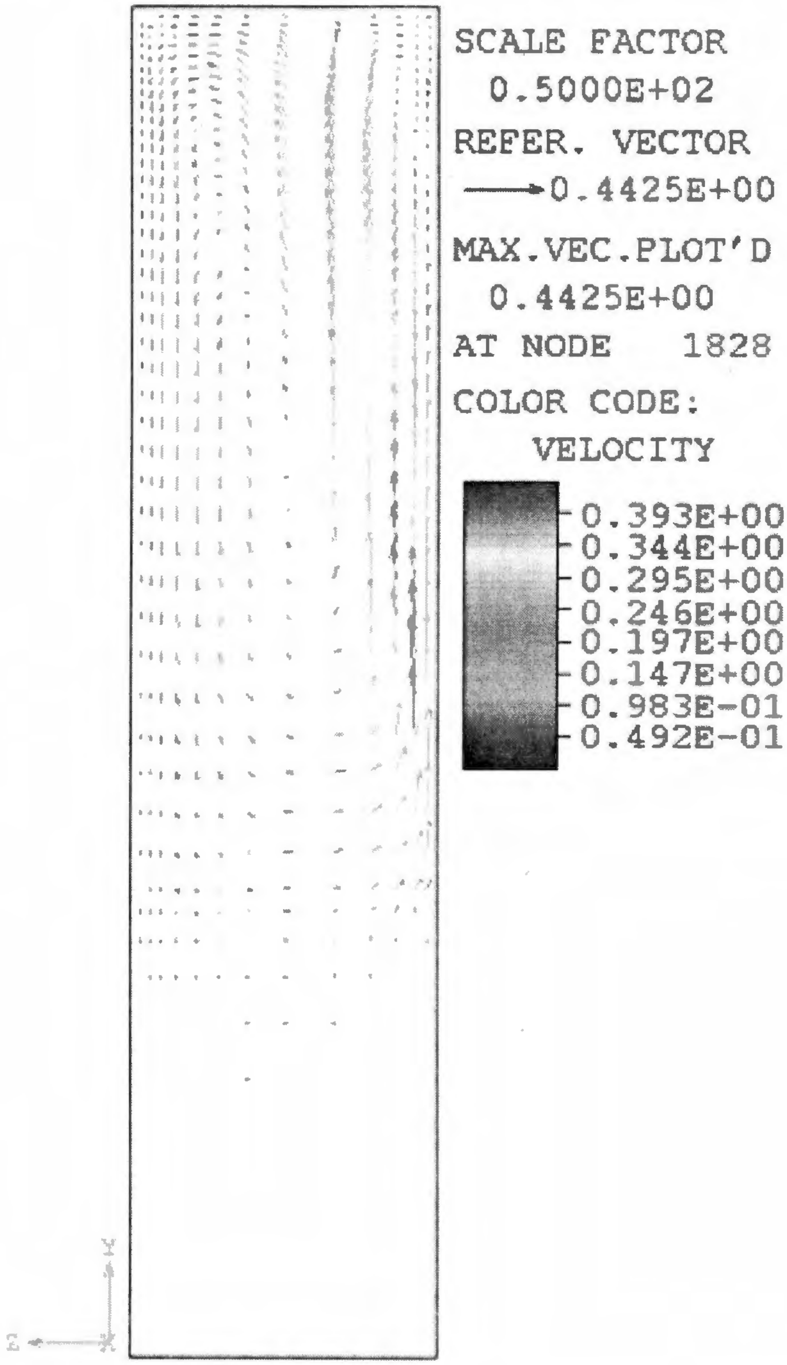

Figure 5.7: Velocity vectors on the symmetry plane with 20mW applied to a 0.5cm diameter spot

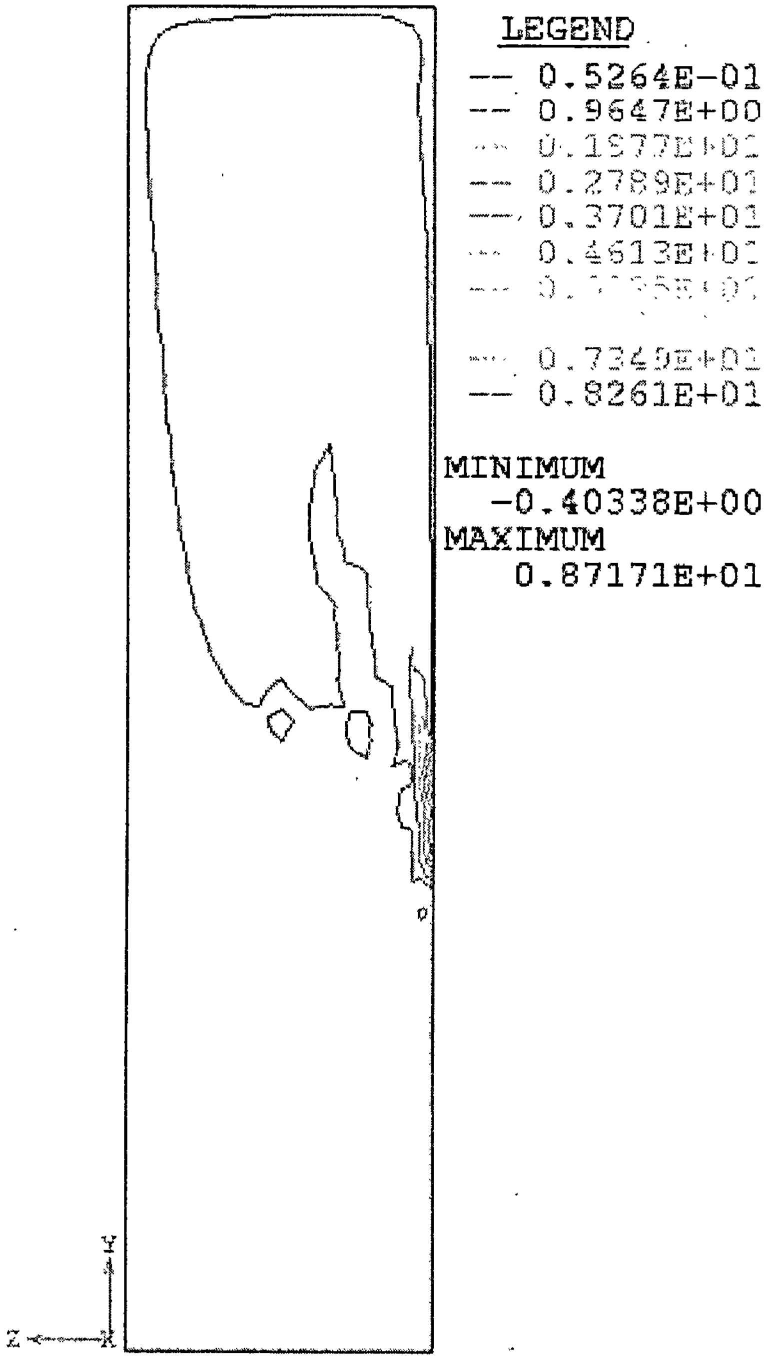

Figure 5.8: Isotherms on the symmetry plane with 30mW applied to a 0.5cm diameter spot

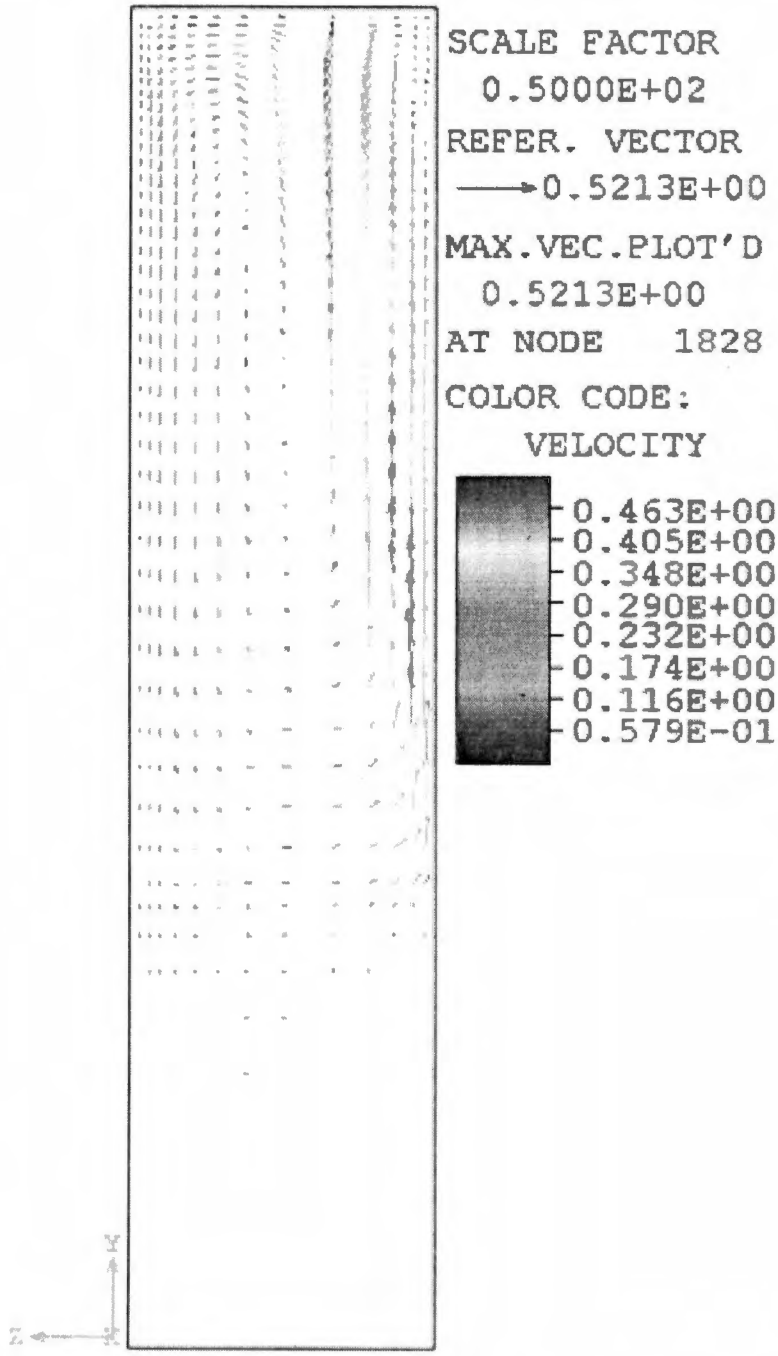

Figure 5.9: Velocity vectors on the symmetry plane with 30mW applied to a 0.5cm diameter spot

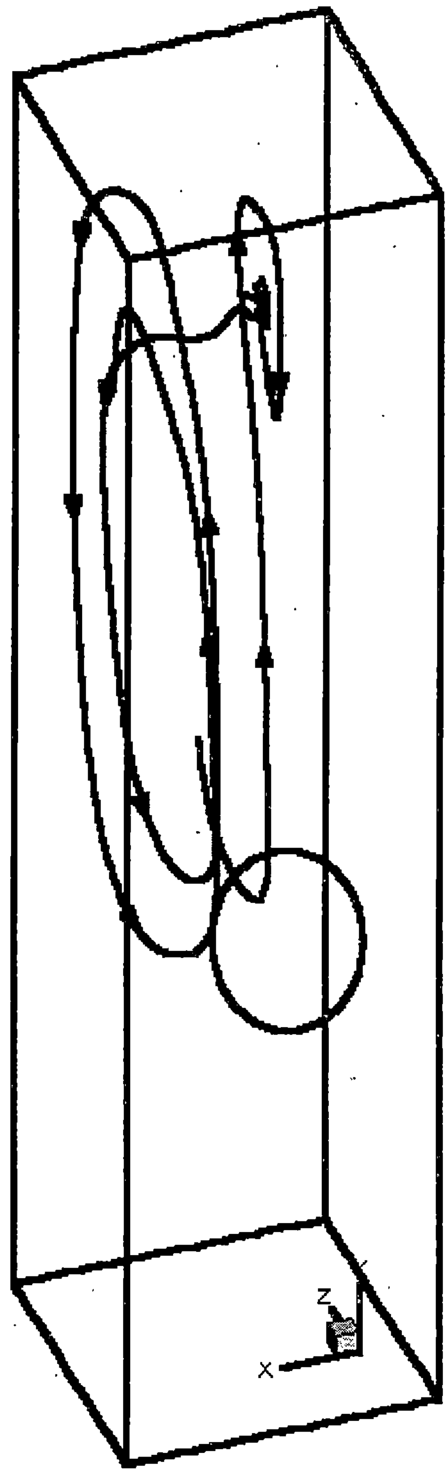

Figure 5.10: Pathline for particle started on the symmetry plane at y=0.25 and z=0.75 with 10mW applied to a 0.5cm diameter spot

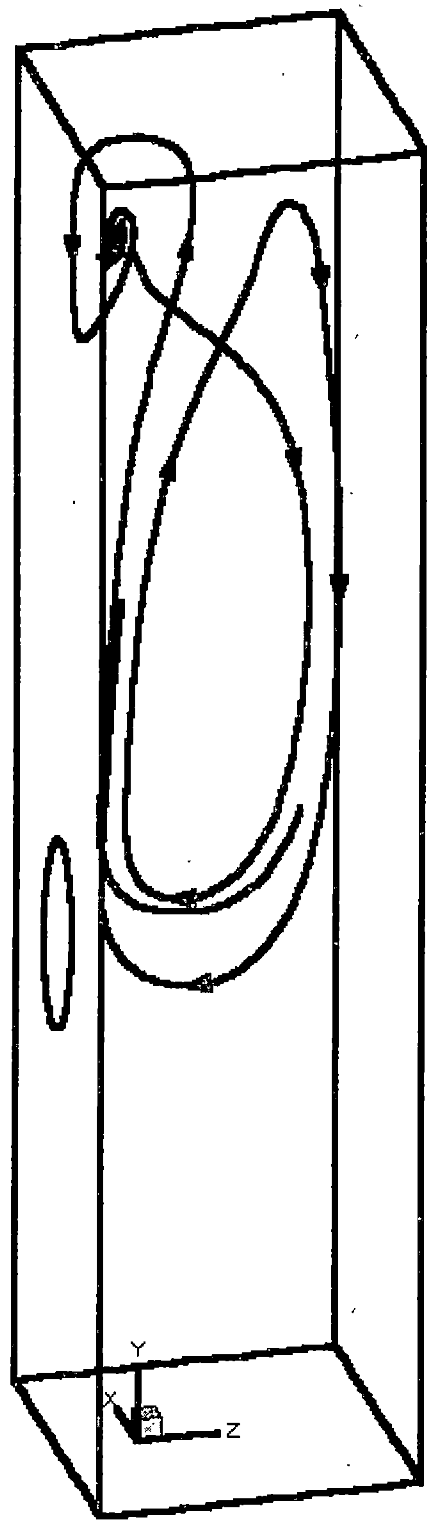

Figure 5.11: Pathline for particle started on the symmetry plane at y=0.25 and z=0.75 with 10mW applied to a 0.5cm diameter spot

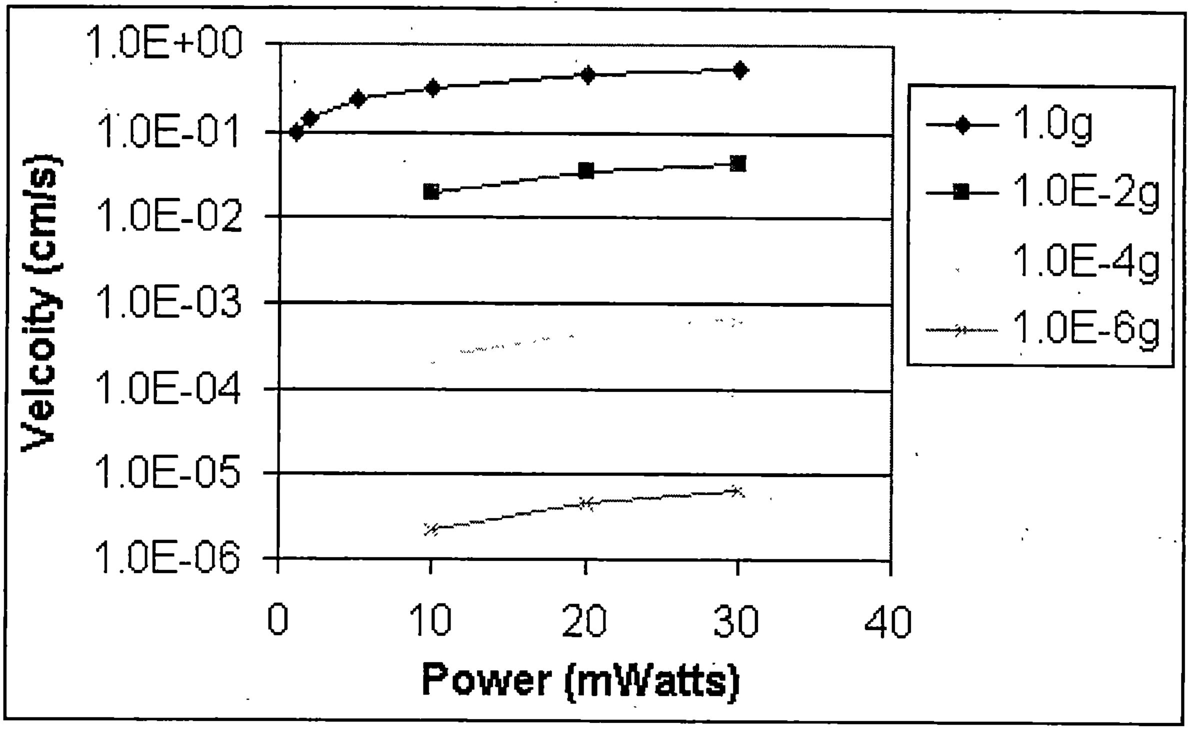

Figure 5.12: Maximum velocity plots for 1g, 1E-2g, 1E-4g, and 1E-6g.

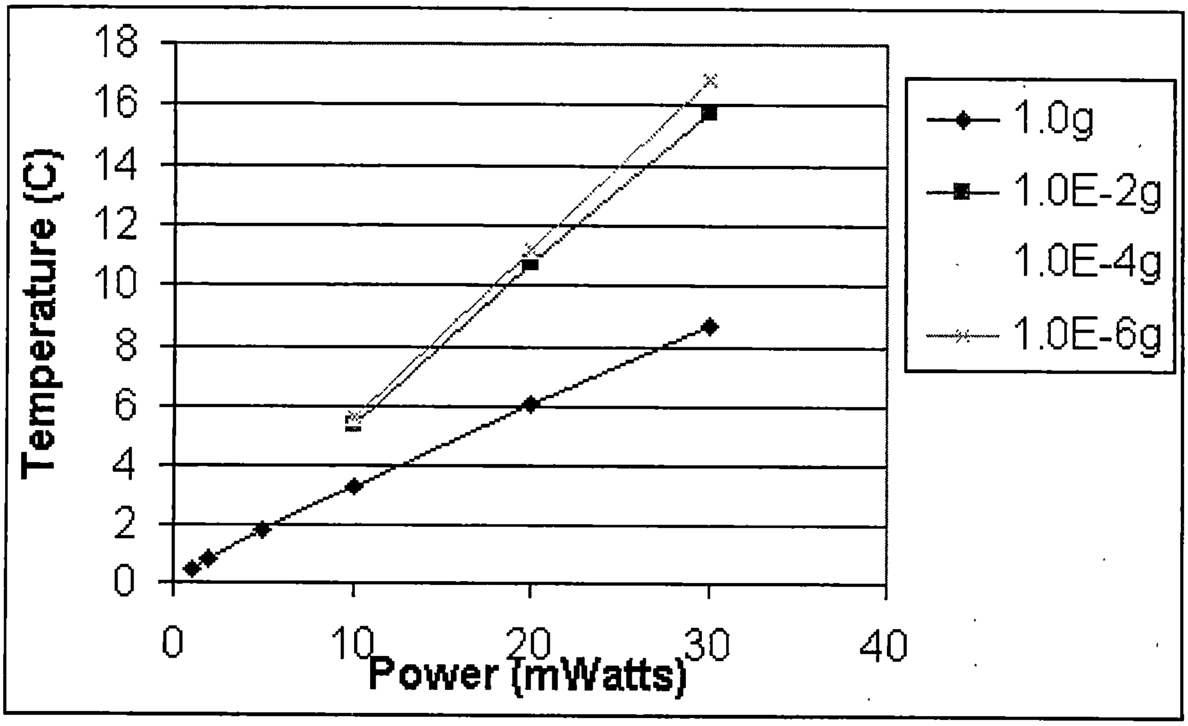

Figure 5.13: Maximum temperature plots for 1g, 1E-2g, 1E-4g, and 1E-6g.

Table 5.1: Maximum velocities($\frac{cm}{s}$) for a side heated rectangular ampule

	1mW	2mW	5mW	10mW	20mW	30mW
1g	9.657E-2	1.449E-1	2.327E-1	3.202E-1	4.425E-1	4.213E-1
1E-2g	n/a	n/a	n/a	2.022E-2	3.473E-2	4.519E-2
1E-4g	n/a	n/a	n/a	2.277E-4	4.554E-4	6.830E-4
1E-6g	n/a	n/a	n/a	6.277E-6	4.555E-6	6.832E-6

Table 5.2: Maximum temperatures(C) for a side heated rectangular ampule

	1mW	2mW	5mW	10mW	20mW	30mW
1g	.4681	0.8480	1.8077	3.3380	6.1239	8.7171
1E-2g	n/a	n/a	n/a	5.417	10.735	15.779
1E-4g	n/a	n/a	n/a	5.613	11.226	16.837
1E-6g	n/a	n/a	n/a	5.613	11.226	16.837

5.1.1 The Side Heating Case

It was evident from figures 5.1 and 5.2 that the side heated case was symmetric about a plane cutting through the center of the heater and extending in the y and z direction. This symmetry plane was used to find the maximum velocity of the flow field. Because the velocity is a function of the amount of heat a fluid particle receives, it seemed obvious that the maximum velocity be found in the symmetry plane and near the top of the heater. This was because the symmetry plane was parallel to the gravity vector and the fluid particle travels a length equal to the diameter of the heater. FIDAP provided a tool to find the maximum velocity and when used it confirmed that assumption. For the 10mW case the maximum velocity of $0.3032\frac{cm}{s}$ is found at node 1828 which is located on the symmetry plane and slightly above the heater. The maximum velocity is used as a metric to compare the strength of the flow from one case to another.

By comparing the vector velocity fields in figures 5.7, 5.9, and 5.11 the strength of the flow field appeared to be strongly dependent on the amount of heat input. This was also evident in the temperature fields. The shape of the flow field, one of the most important contributors to degradation of crystal quality, was strongly governed by heat input. As the heat input increased the primary circulation zone moved toward the top of the ampule. Another interesting feature was the formation of a small recirculation area above and to the left of the main zone. This was likely formed from the higher velocity fluid elements that came out of the symmetry plane region of the heater, e.g. the fastest moving fluid, which then interacted with the wall. This feature was better visualized in figures 5.4 and 5.5 where it appeared as a small cell of rotating fluid near the top and centered on the symmetry plane. As the heat input increased this secondary zone was forced closer to the wall as observed in figures 5.7, 5.9, and 5.11. This behavior was evident from the temperature contours as well. Based on the trend seen in the 10 to 30mW range it appeared that this behavior was only due to the temperature gradient penetration. As the circulation intensity increased it appeared that this zone would die out.

One difficult problem in numerical simulations is to know how much of the solution is physically valid and how much is approximation error. The jaggedness of the isotherms is most likely an artifact of approximation error. This could be verified by refining the mesh to see if this feature is reduced. While this feature is obvious, it probably is not critical. Since there was no control over the interval between isotherms some of the isotherms could be within the numerical error. It is for this reason that it is doubtful that the 0.04927°C interval in figure 5.6 and the 0.05264°C interval in figure 5.8 are physically real since this isotherm reperesents only 1% of the largest interval. It is more necessary to compare the overall results to the physical case to see if the main features are in agreement.

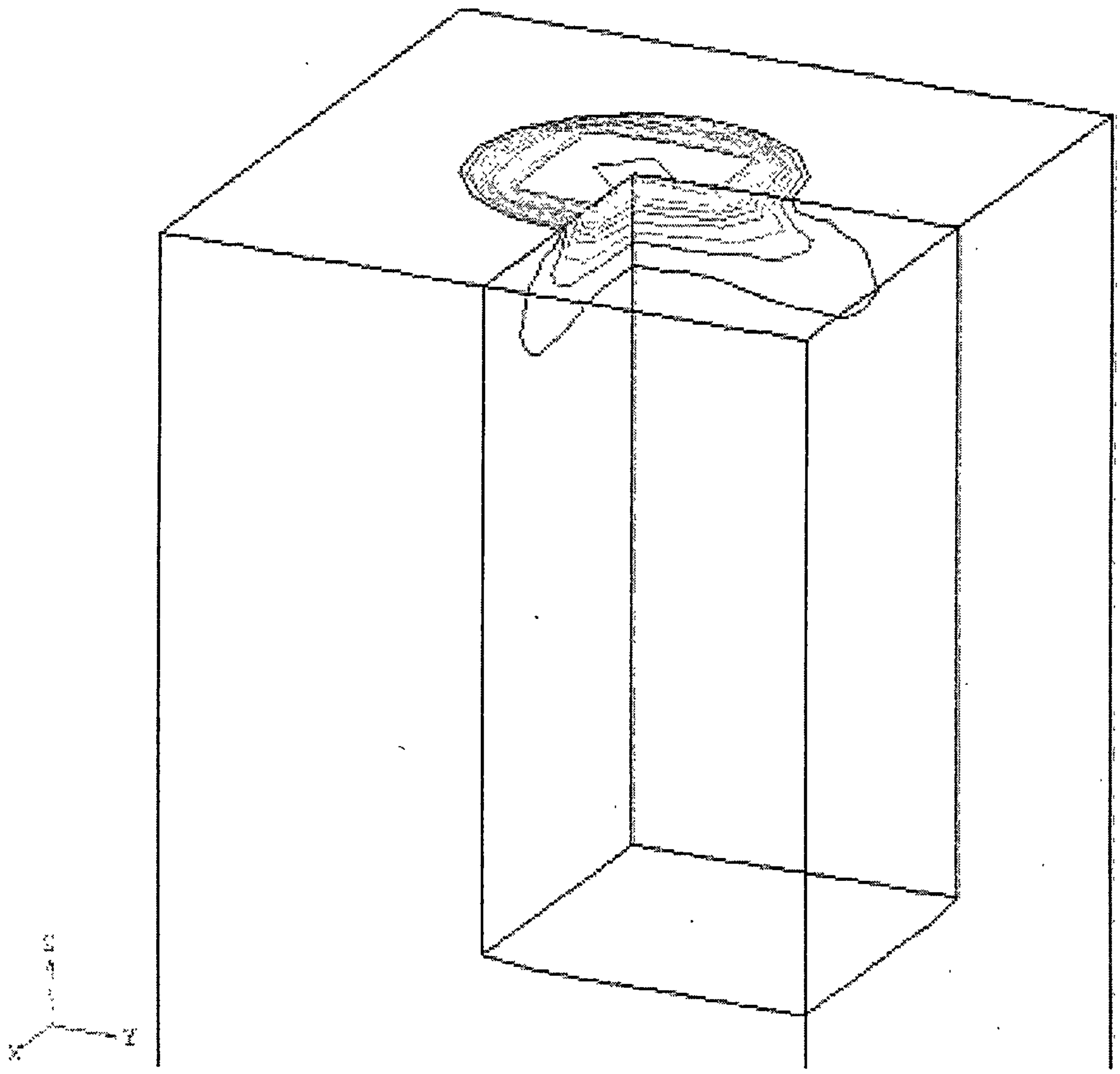

Figure 5.14: Isotherms as viewed with a corner section removed for the 10mW top heated case

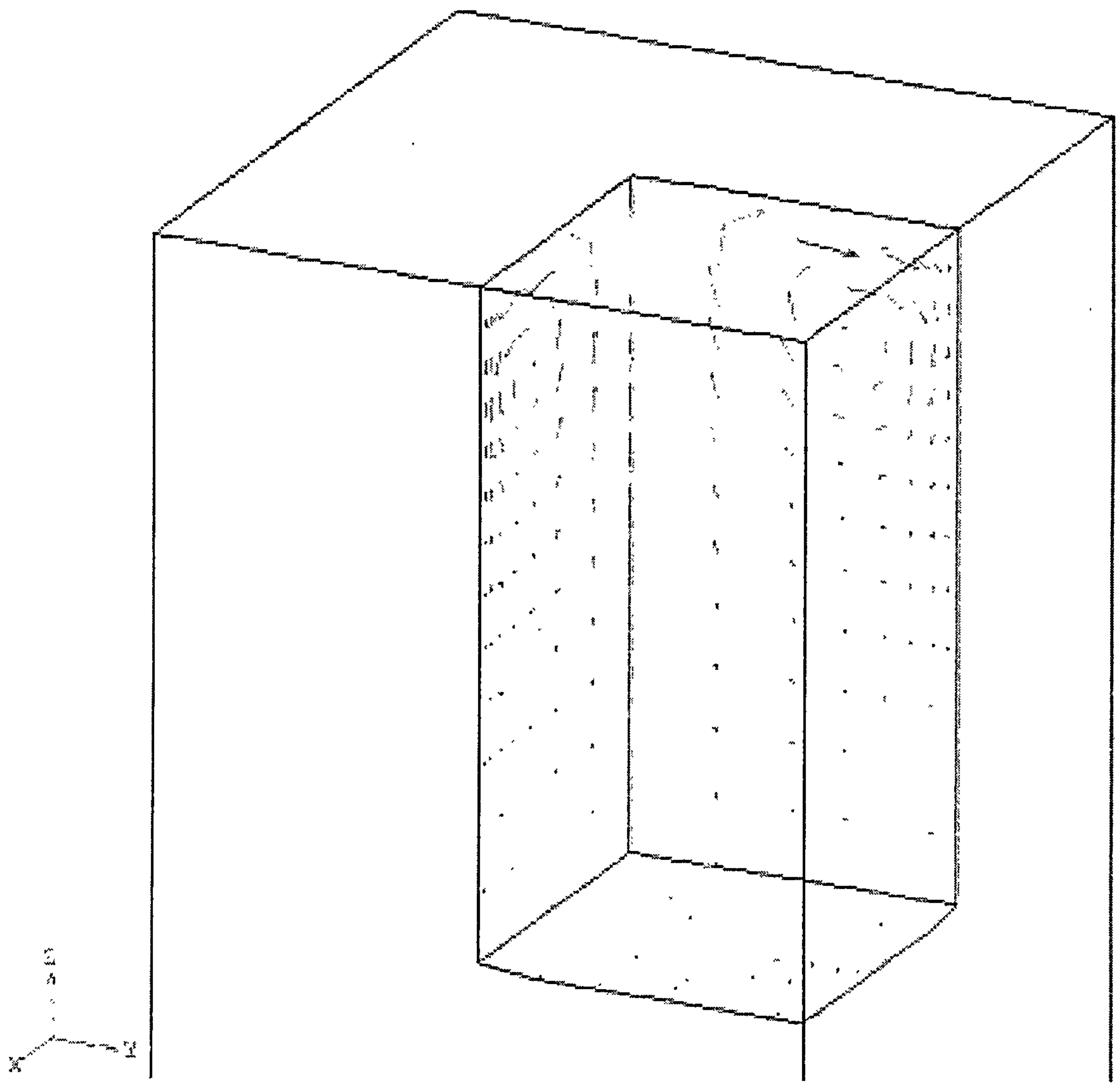

Figure 5.15: Velocity vectors as viewed with a corner section removed for the 10mW top heated case

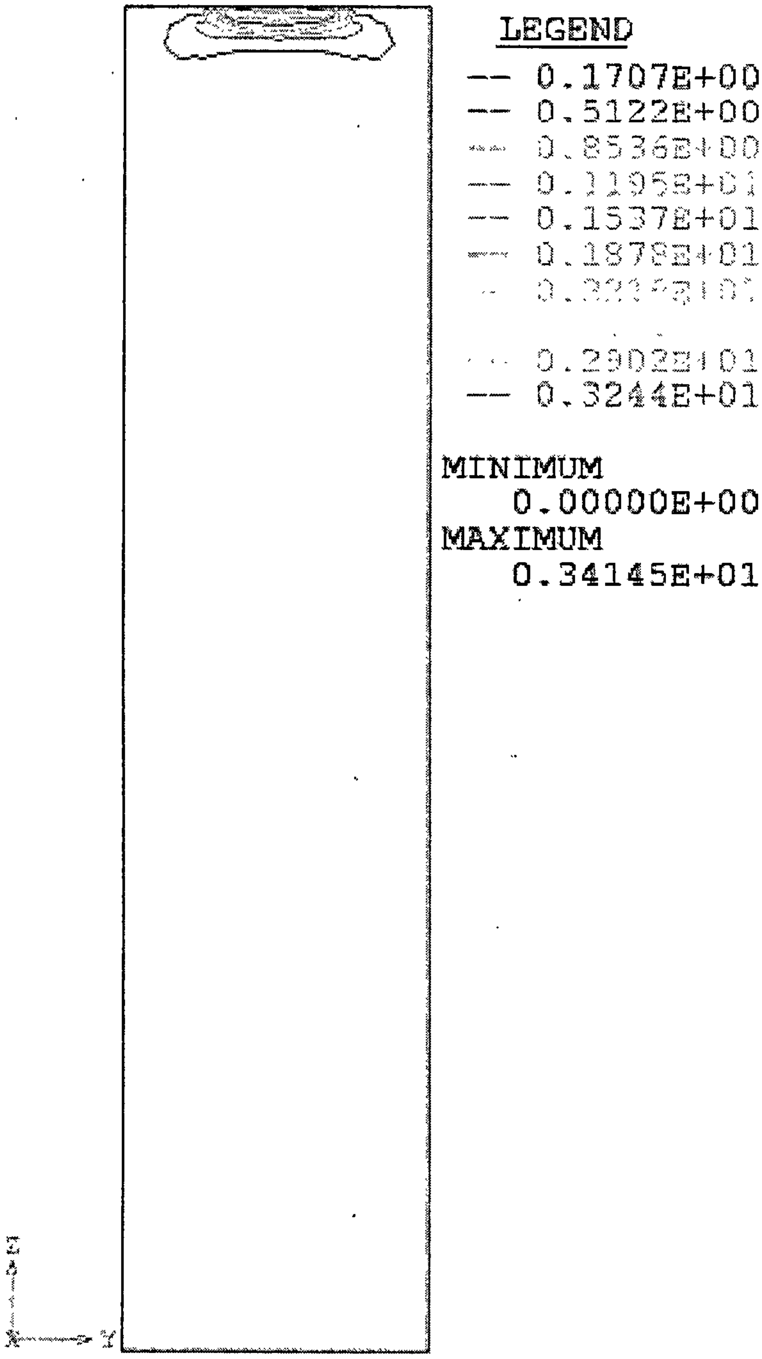

Figure 5.16: Isotherms on the symmetry plane with 10mW applied to a 0.5cm diameter top spot heater

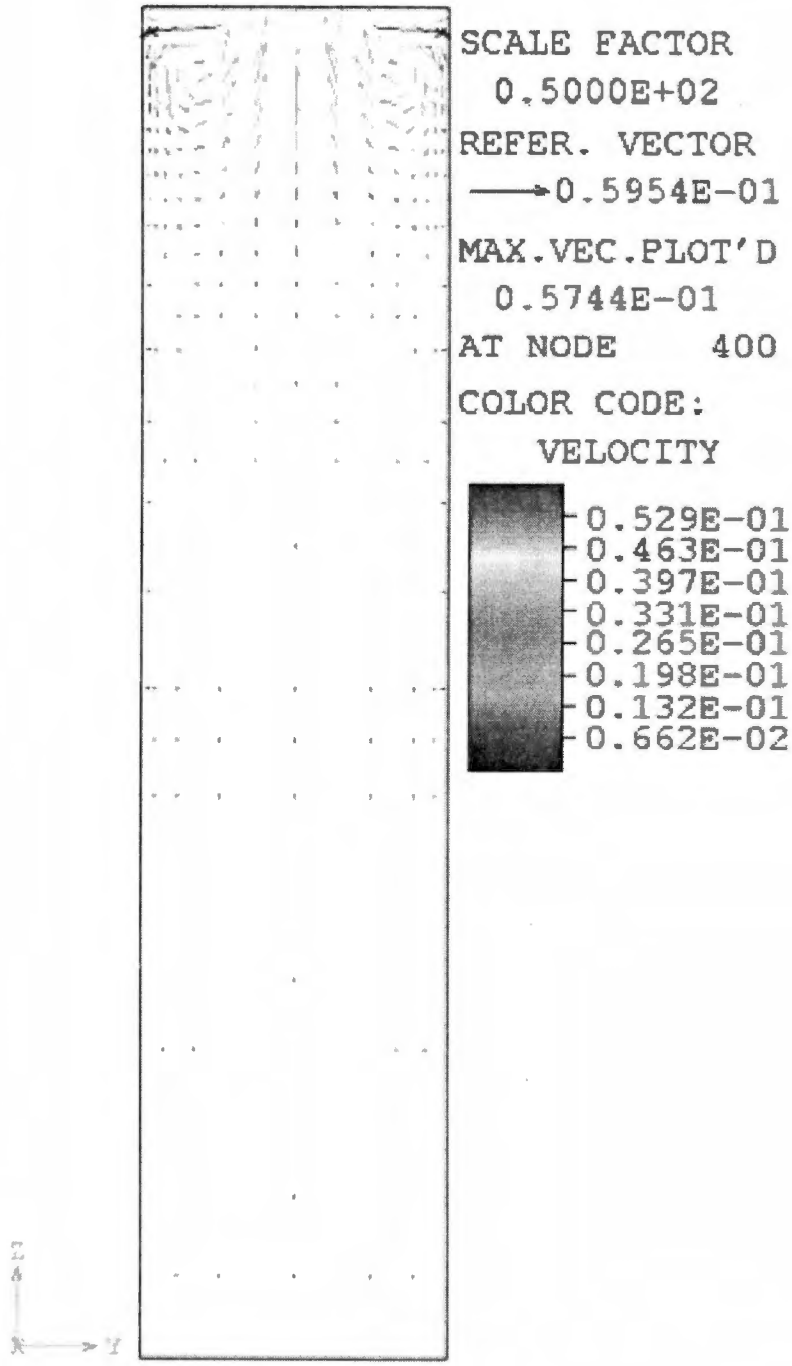

Figure 5.17: Velocity vectors on the symmetry plane with 10mW applied to a 0.5cm diameter top spot heater

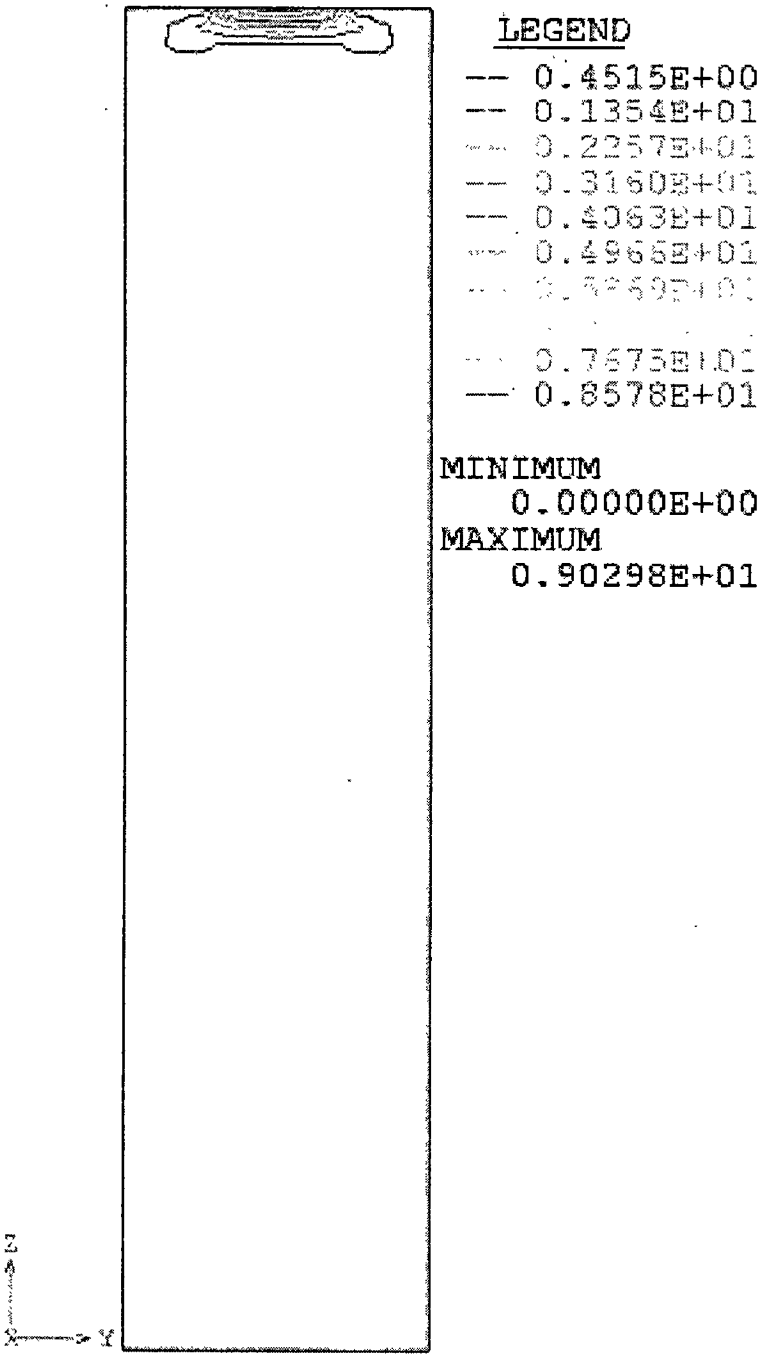

Figure 5.18: Isotherms on the symmetry plane with 20mW applied to a 0.5cm diameter top spot heater

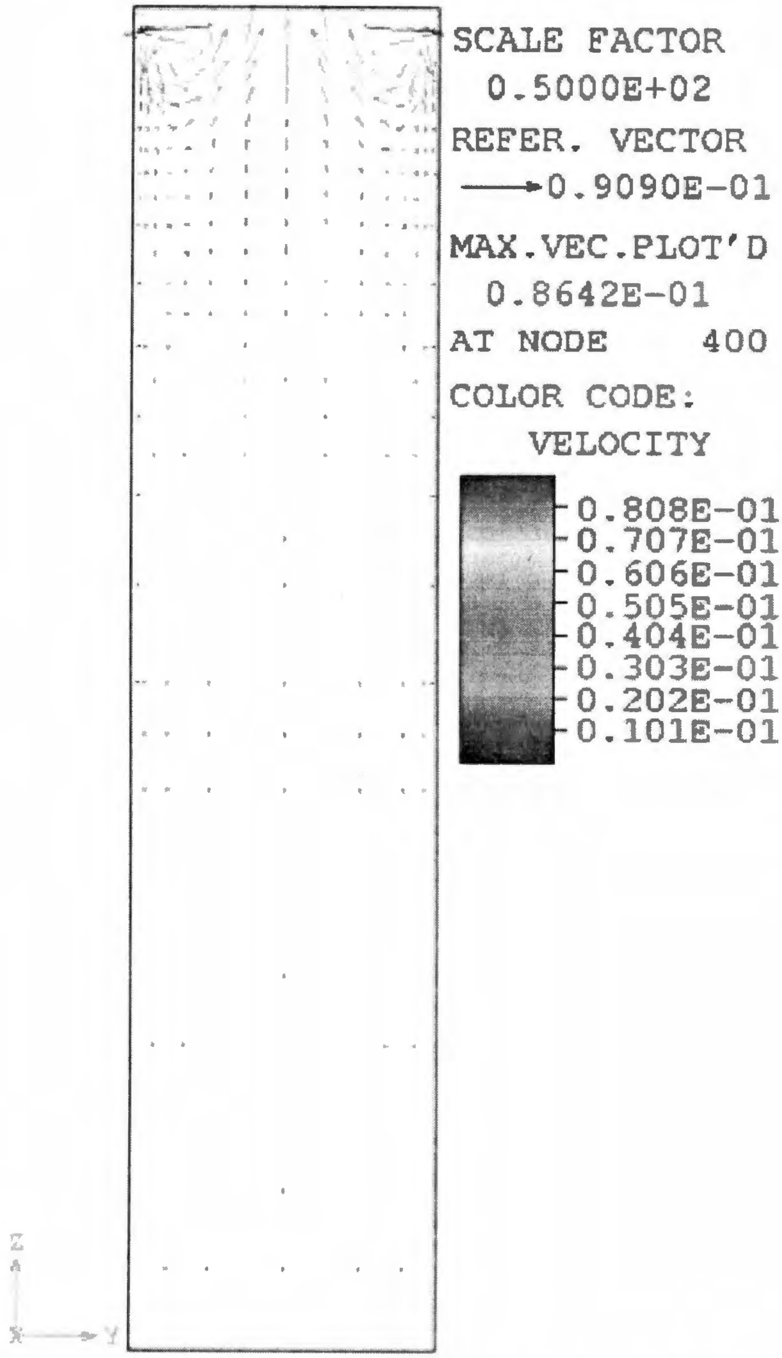

Figure 5.19: Velocity vectors on the symmetry plane with 20mW applied to a 0.5cm diameter top spot heater

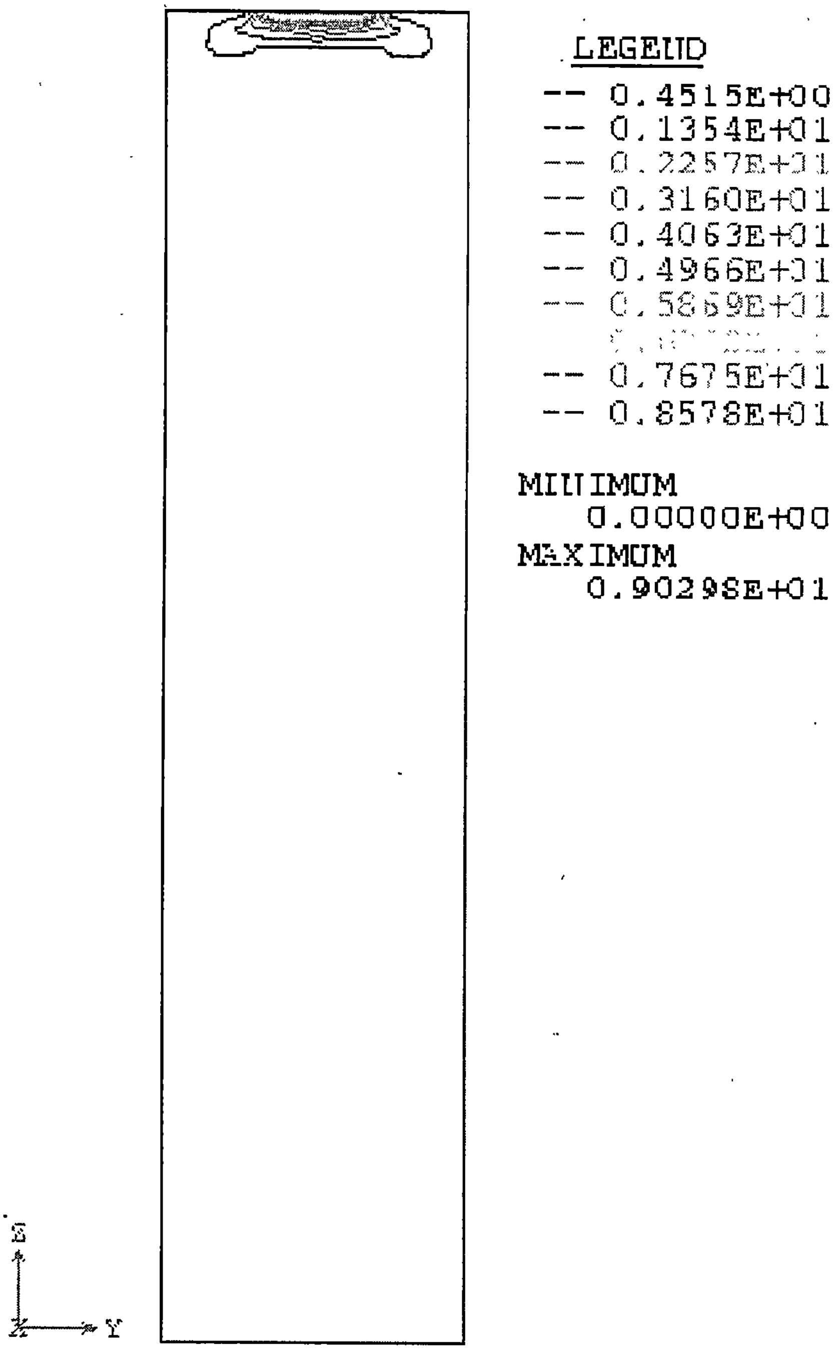

Figure 5.20: Isotherms on the symmetry plane with 30mW applied to a 0.5cm diameter top spot heater

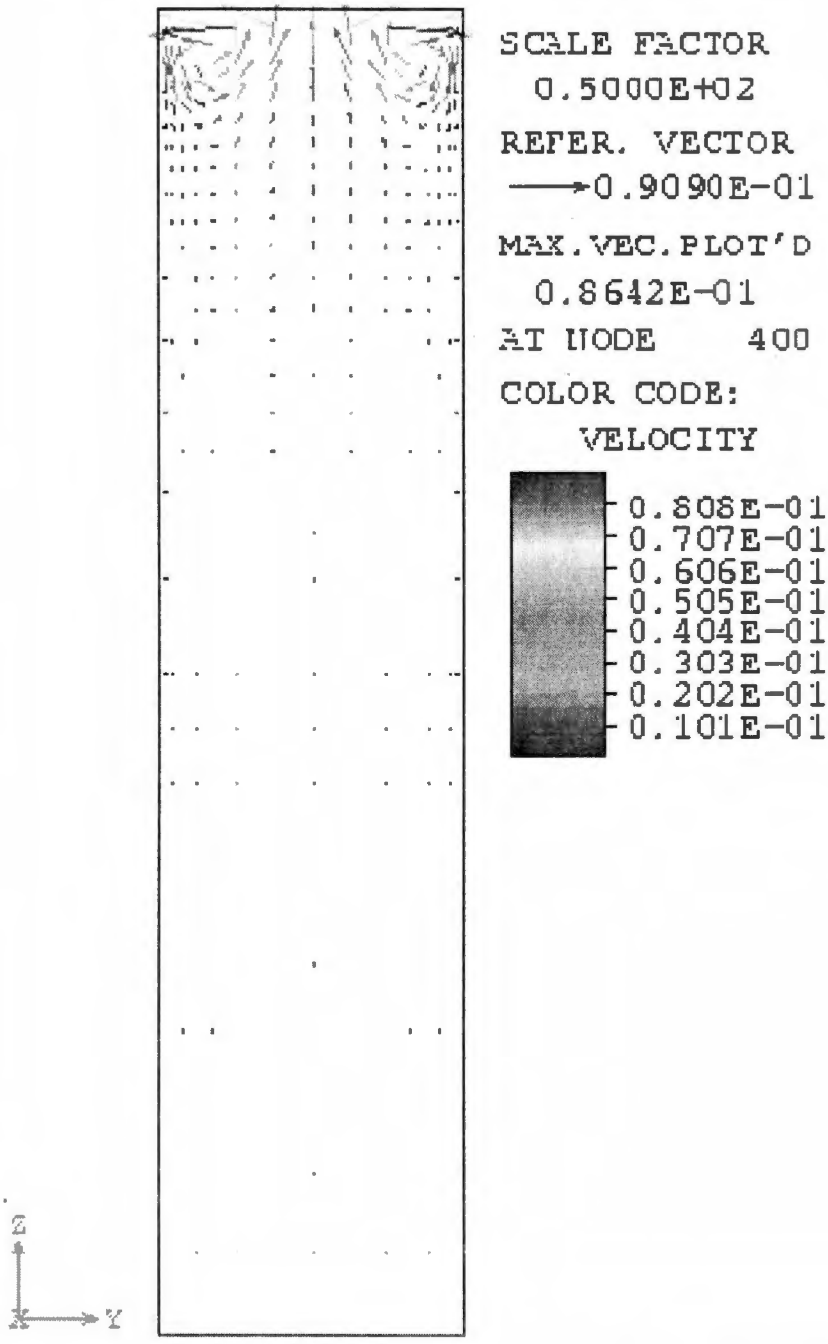

Figure 5.21: Velocity vectors on the symmetry plane with 30mW applied to a 0.5cm diameter top spot heater

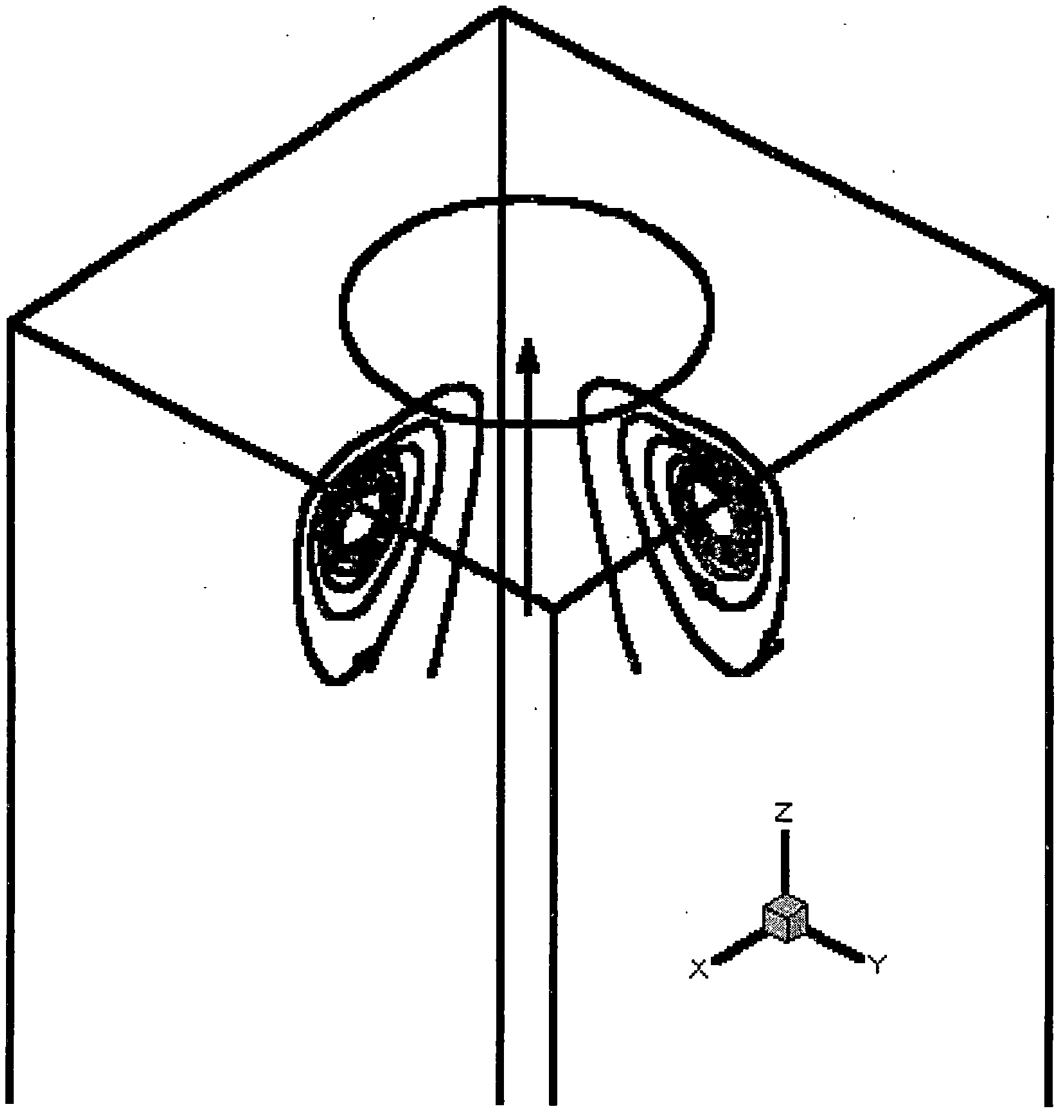

Figure 5.22: Pathlines for the 10mW top heated case

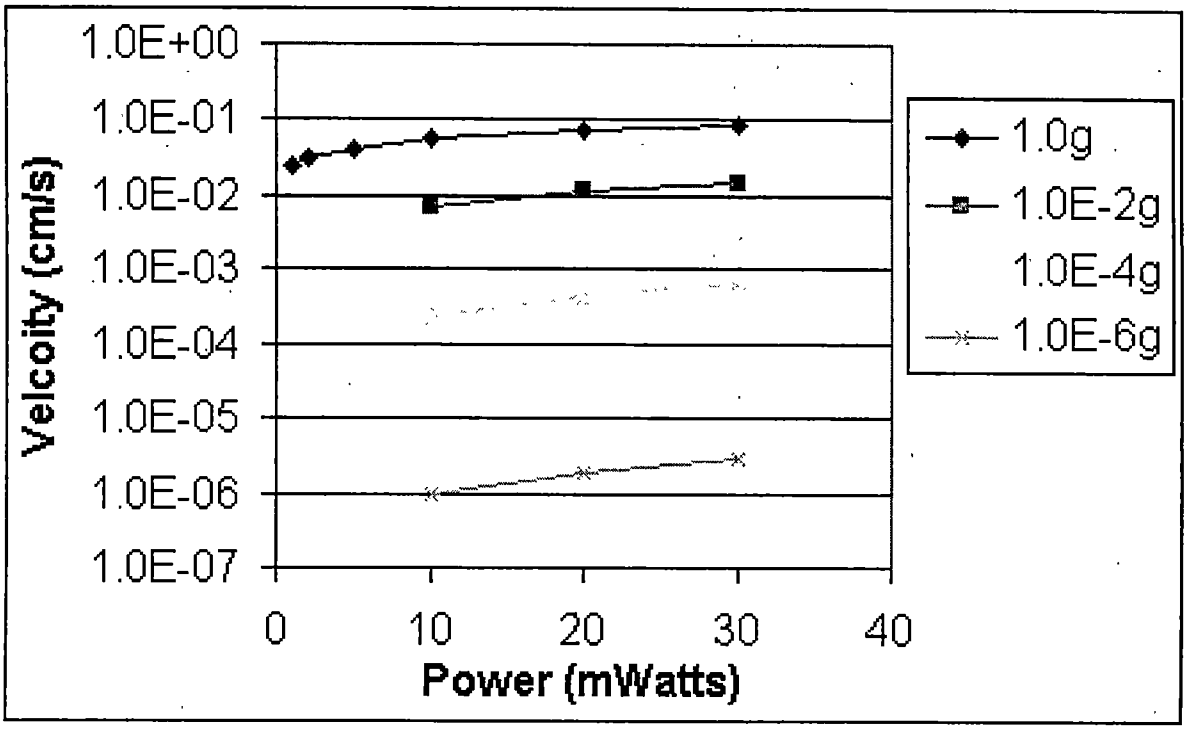

Figure 5.23: Maximum velocity plots for 1g, 1E-2g, 1E-4g, and 1E-6g.

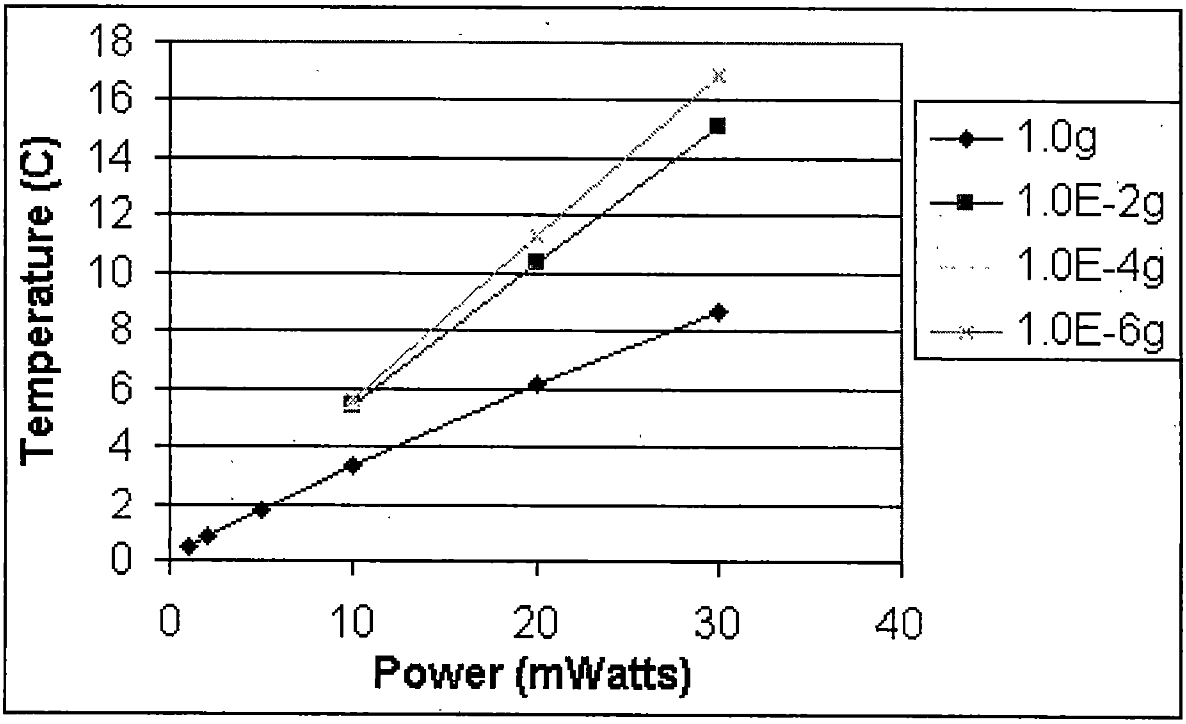

Figure 5.24: Maximum temperature plots for 1g, 1E-2g, 1E-4g, and 1E-6g.

Table 5.3: Maximum velocities($\frac{cm}{s}$) for a side heated trapezoidal ampule

	1mW	2mW	5mW	10mW	20mW	30mW
1g	2.486E-2	3.092E-2	4.260E-2	5.744E-2	7.493E-2	8.642E-2
1E-2g	n/a	n/a	n/a	7.030E-3	1.132E-2	1.446E-2
1E-4g	n/a	n/a	n/a	9.343E-5	1.864E-4	2.785E-4
1E-6g	n/a	n/a	n/a	9.397E-7	1.875E-6	2.812E-6

Table 5.4: Maximum temperatures(C) for a top heated ampule

	1mW	2mW	5mW	10mW	20mW	30mW
1g	.4404	0.8087	1.8303	3.4145	6.3188	9.0298
1E-2g	n/a	n/a	n/a	5.3950	10.394	15.106
1E-4g	n/a	n/a	n/a	5.6292	11.254	16.8793
1E-6g	n/a	n/a	n/a	5.6317	11.263	16.895

5.1.2 The Top Heating Case

When the ampule was heated from the top it was also strongly dominated by symmetry, more than even the side heating case. This was evident in both figure 5.14, figure 5.15 where there is symmetry along three planes. Although there are mathematically an infinite number of symmetry planes to chose in this case, it seemed evident from the analysis that one which cuts through the center of the heater and ran the length of the ampule parallel to the gravity vector would show the full character of the flow. Choosing the angle of the plane to the x and y axis was then an arbitrary choice.

By analyzing figures 5.16, 5.18, and 5.20 it was evident that the maximum velocity of the flow was strongly correlated to the heat input. This also held for the maximum temperature. A strong circulation formed around the heat input area. This region was torus shaped, at the top of the ampule, and centered on the heater. This behavior was due to the heating of the fluid elements near the center which would rise towards the top of the ampule. The fluid they displaced would be pushed out towards the outer walls and be cooled. As the elements cooled they would sink. This behavior is similar to what one would find in a Benard convection cell[20].

The shape of this torus does not vary much with the heat input. The velocities seen in this configuration were much lower than the side heating cases and this may have been due to wall friction. The main flow area interacts with the wall more than the side heating case because the bulk of the flow motion was always within 0.5cm from a wall. The fluid mixing was much less in this case as was evident in the penetration of the isotherms.

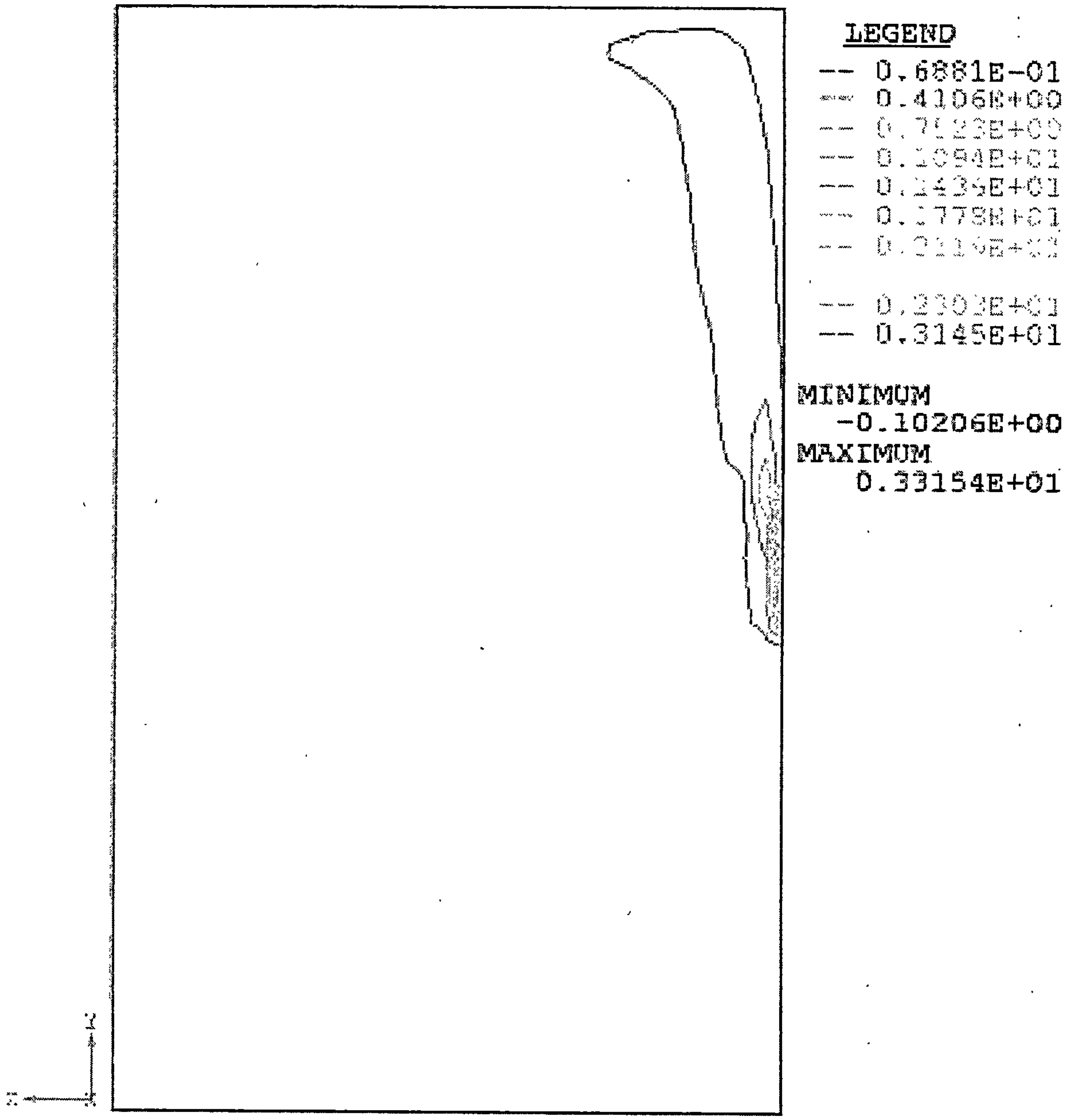

Figure 5.25: Isotherms on the symmetry plane with 10mW applied to a 0.5cm diameter spot

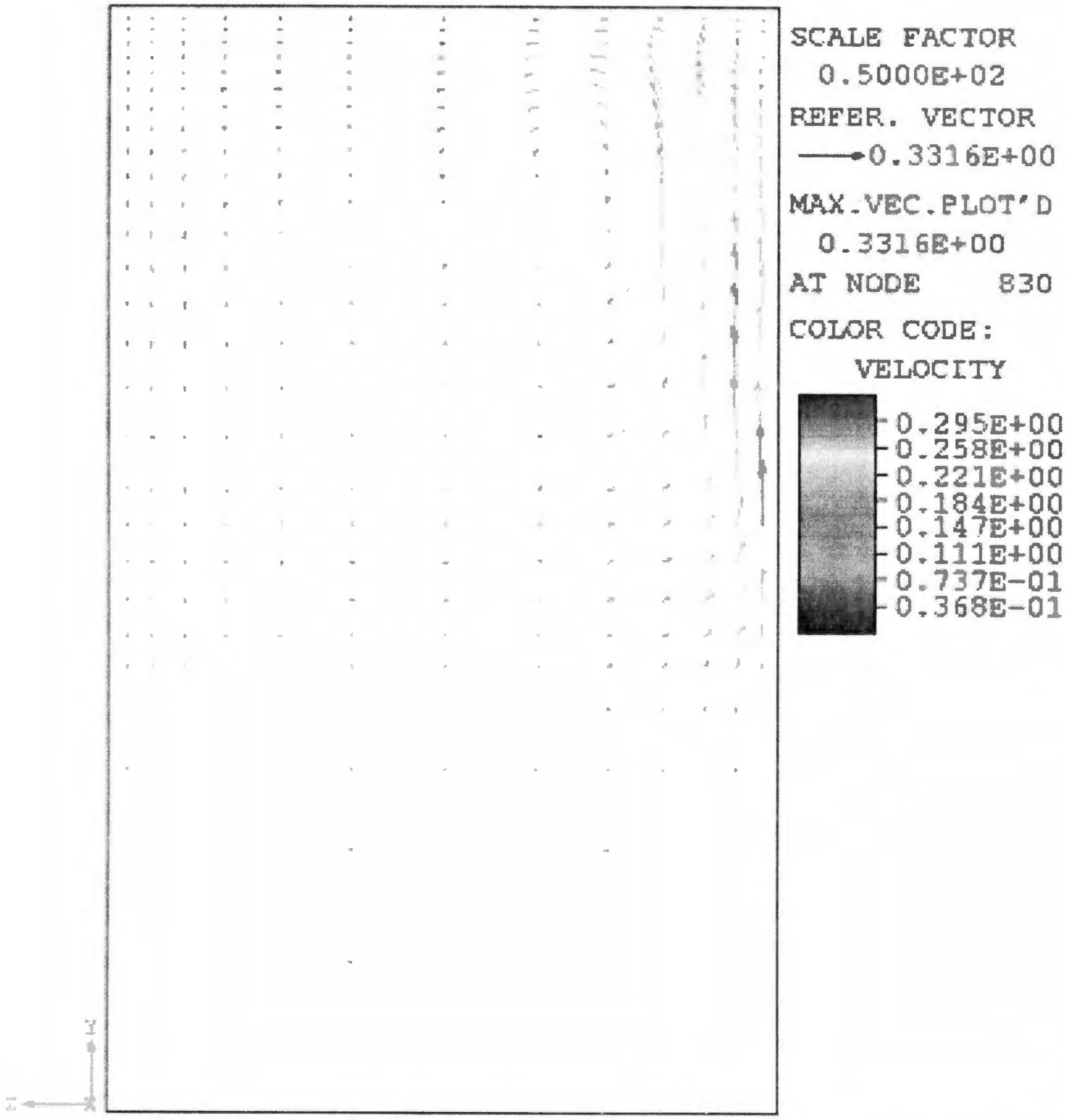

Figure 5.26: Velocity vectors on the symmetry plane with 10mW applied to a 0.5cm diameter spot

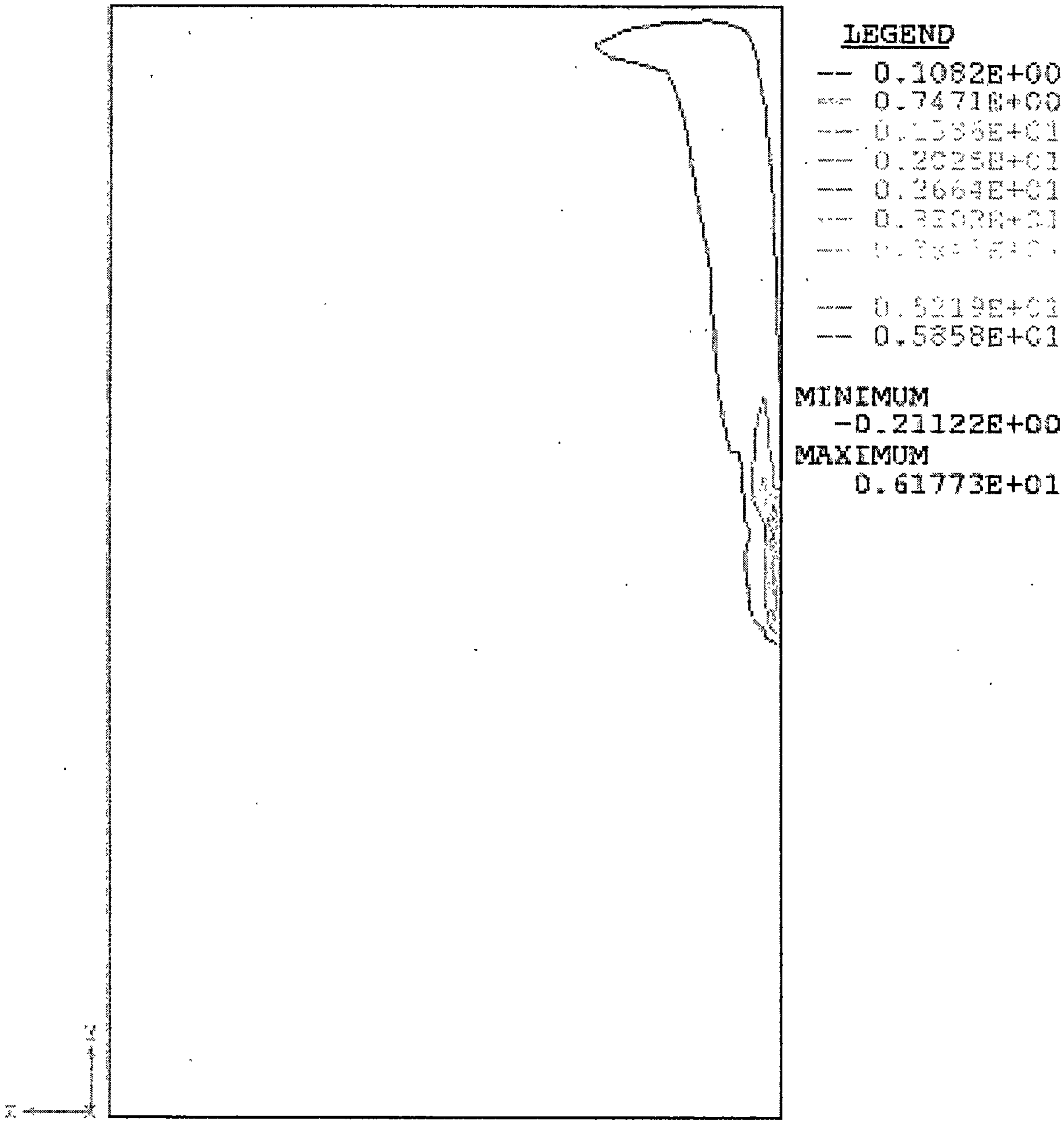

Figure 5.27: Isotherms on the symmetry plane with 20mW applied to a 0.5cm diameter spot

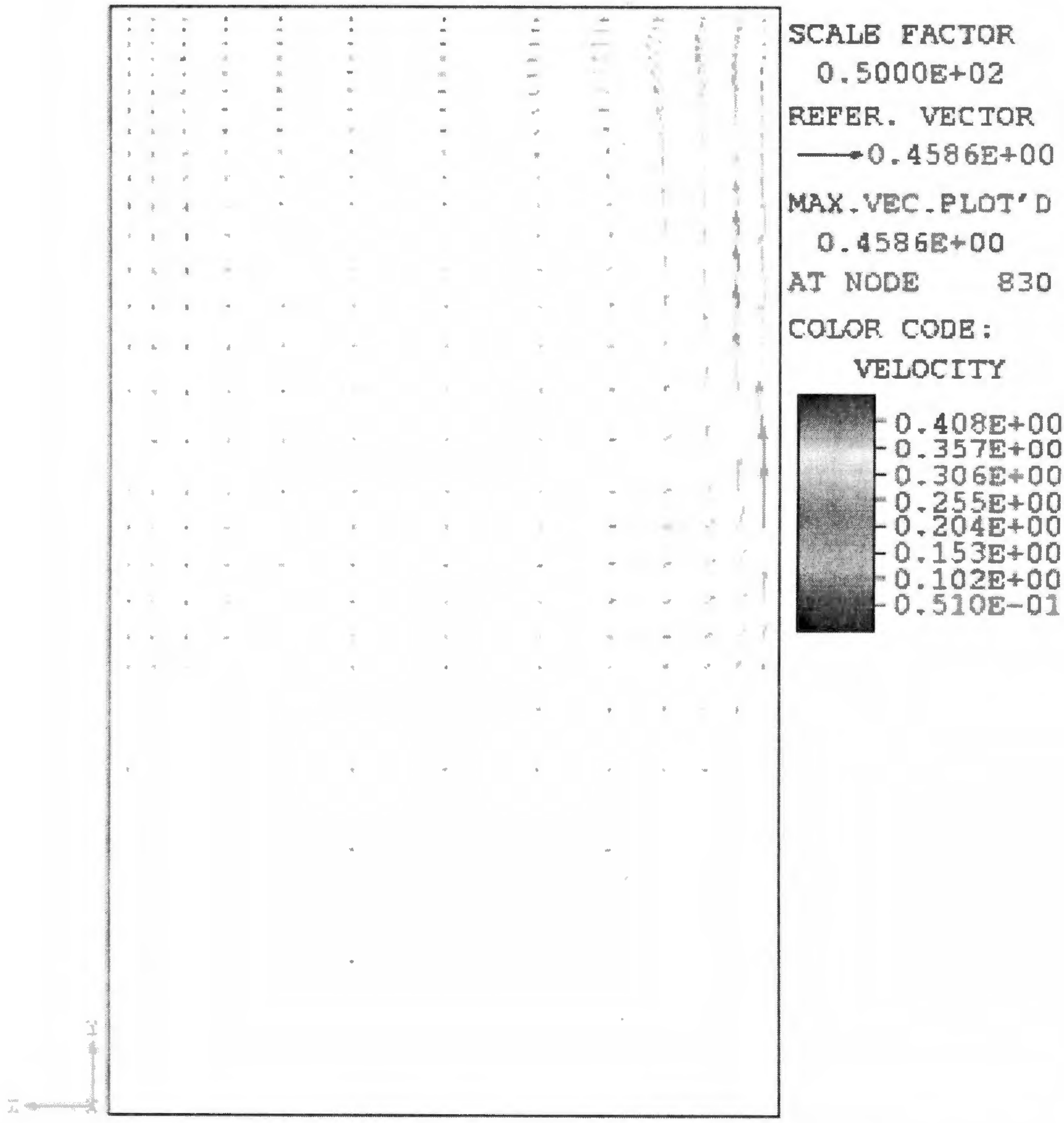

Figure 5.28: Velocity vectors on the symmetry plane with 20mW applied to a 0.5cm diameter spot

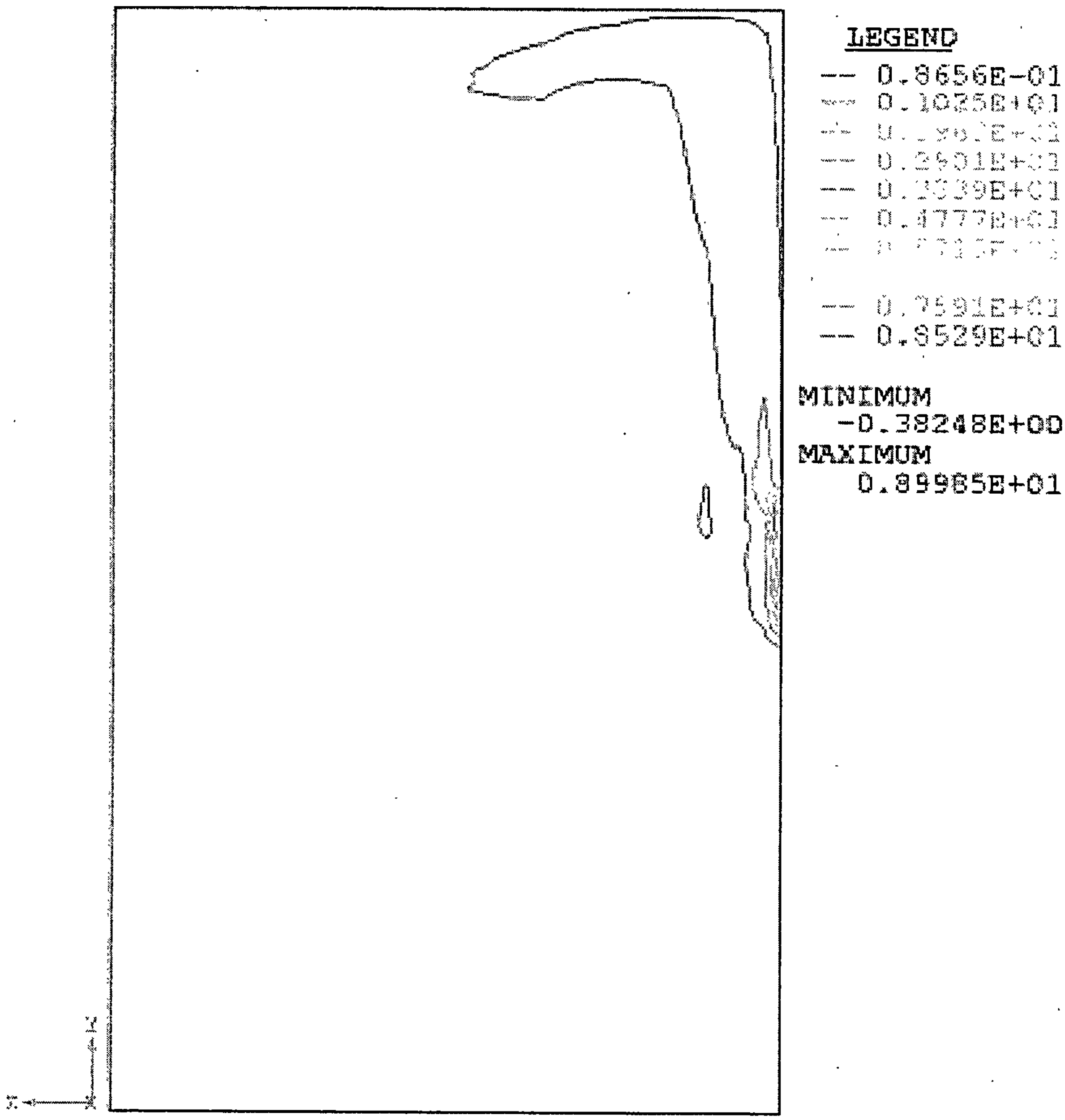

Figure 5.29: Isotherms on the symmetry plane with 30mW applied to a 0.5cm diameter spot

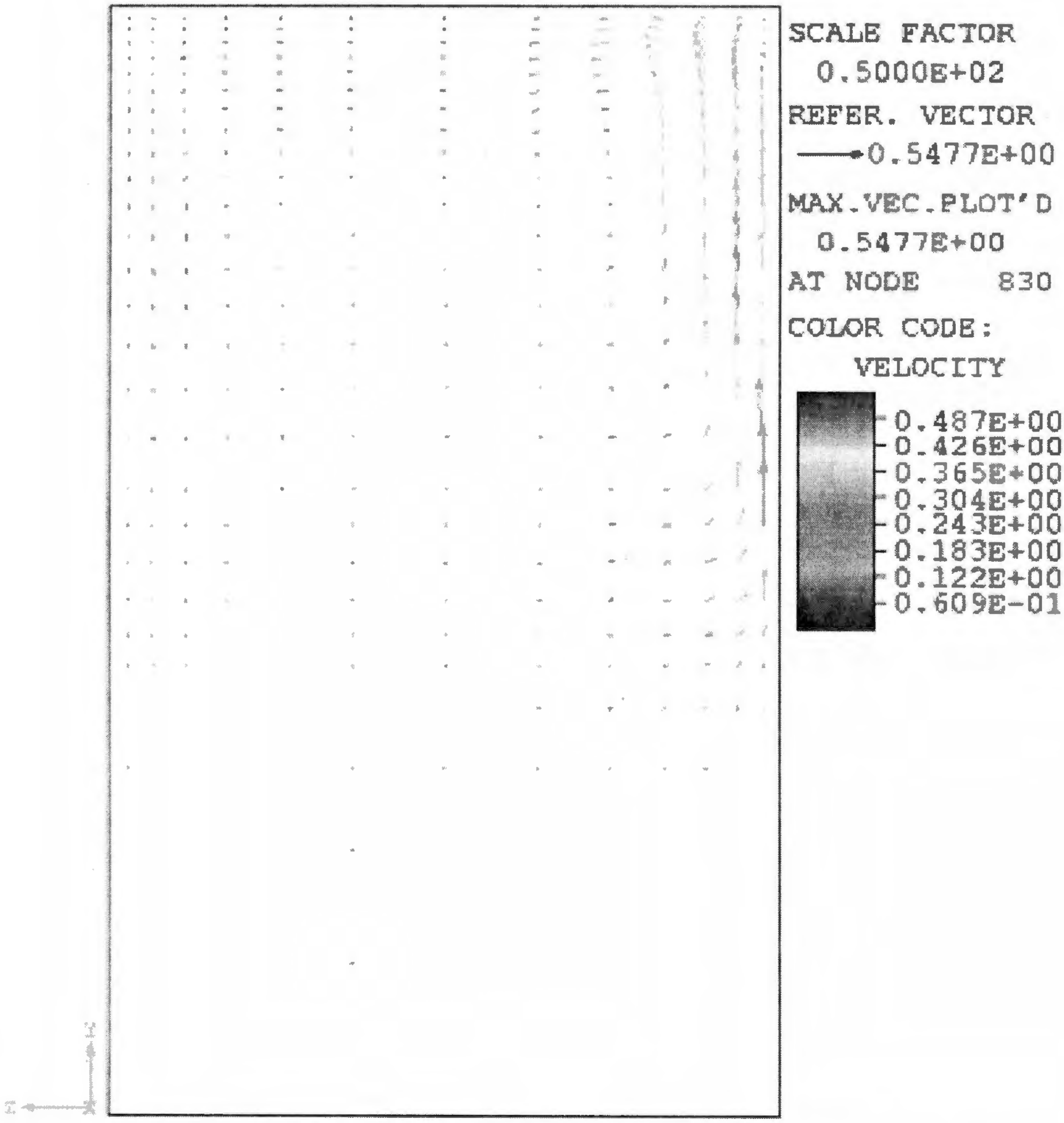

Figure 5.30: Velocity vectors on the symmetry plane with 30mW applied to a 0.5cm diameter spot

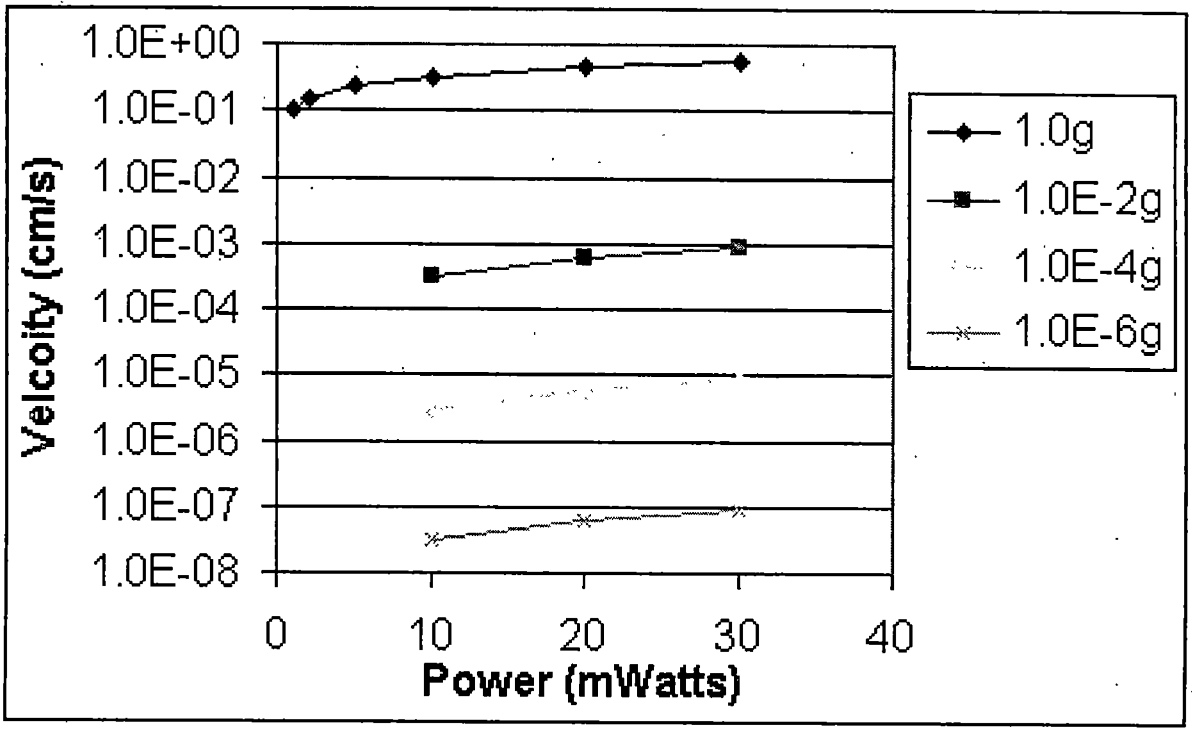

Figure 5.31: Maximum velocity plots for 1g, 1E-2g, 1E-4g, and 1E-6g.

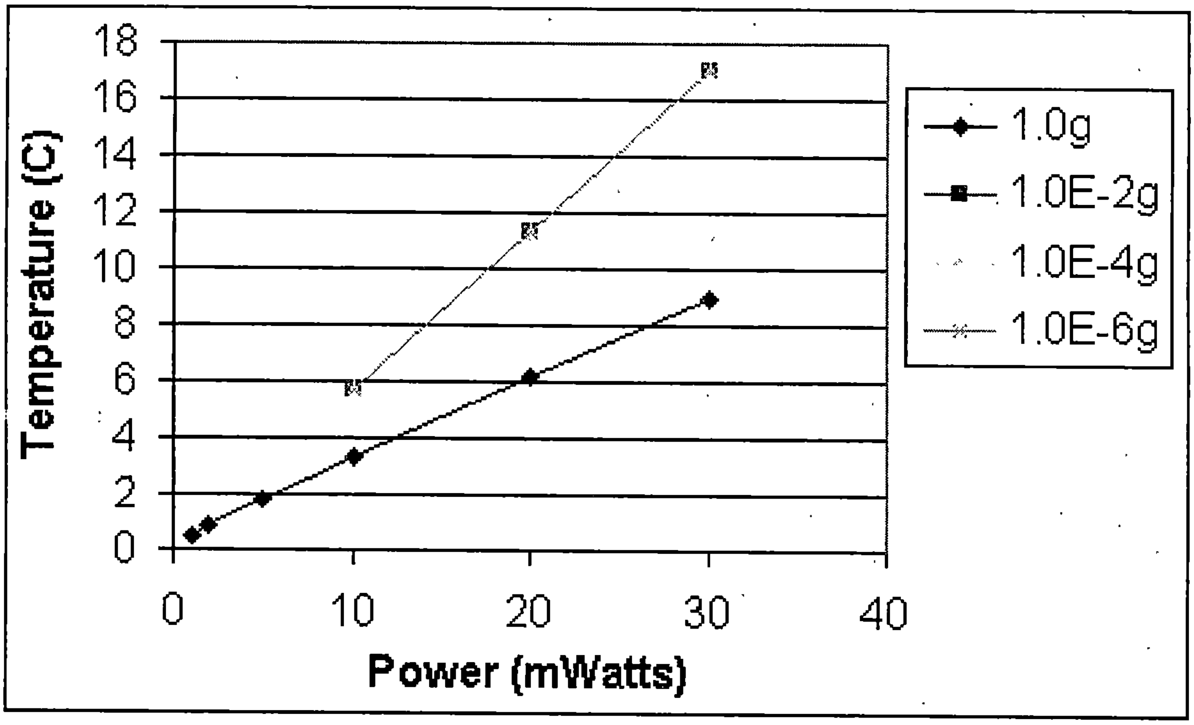

Figure 5.32: Maximum temperature plots for 1g, 1E-2g, 1E-4g, and 1E-6g.

Table 5.5: Maximum velocities($\frac{cm}{s}$) for a side heated trapezoidal ampule

	1mW	2mW	5mW	10mW	20mW	30mW
1g	1.046E-1	1.544E-1	2.348E-1	3.316E-1	4.586E-1	5.477E-1
1E-2g	n/a	n/a	n/a	2.022E-2	3.473E-2	4.519E-2
1E-4g	n/a	n/a	n/a	2.277E-4	4.554E-4	6.830E-4
1E-6g	n/a	n/a	n/a	6.277E-6	4.555E-6	6.832E-6

Table 5.6: Maximum temperatures(C) for a side heated trapezoidal ampule

	1mW	2mW	5mW	10mW	20mW	30mW
1g	.4404	0.8087	1.8303	3.3154	6.1773	8.9985
1E-2g	n/a	n/a	n/a	5.417	10.735	15.779
1E-4g	n/a	n/a	n/a	5.613	11.226	16.837
1E-6g	n/a	n/a	n/a	5.613	11.226	16.837

5.2 Trapezoidal Ampule

The side heated trapezoidal ampule was also dominated by the same symmetry plane as the side heated rectangular ampule. This provided insight as to where the areas of interest were. Comparing the two ampules the trapezoidal ampule achieved slightly higher maximum temperature and velocity although the location of these were in similar spots. This may have been due to the higher volume of fluid in the trapezoidal ampule, $7.5cm^3$ as compared to $4cm^3$. Given the higher volume of fluid and a more open container, the fluid will gain a higher momentum which would offset the additional viscous forces of a container with more surface area.

One feature that is noticeably absent is the small recirculating region that was evident in the rectangular case. One explanation was that the isotherms were closer to the wall in the trapezoidal case, especially in the lower powered case. This decreases the area of the dead zone that sits in the top right corner of the velocity and temperature cuts.

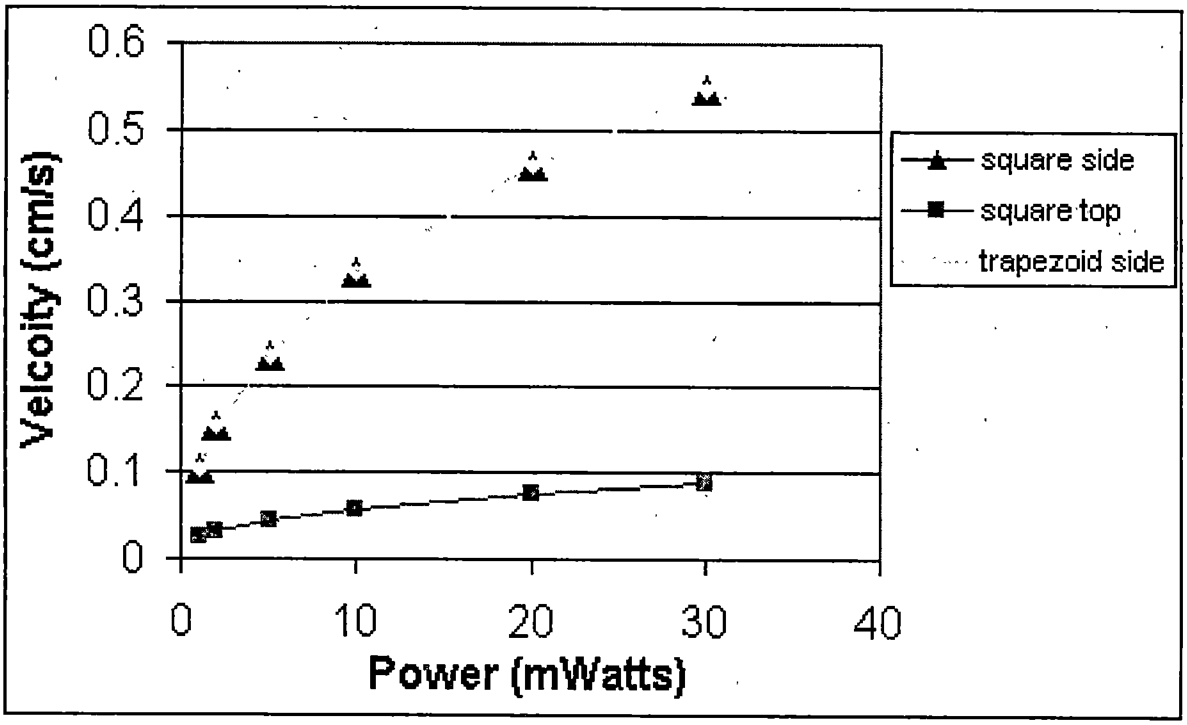

Figure 5.33: Maximum velocity plots for three ampule configurations.

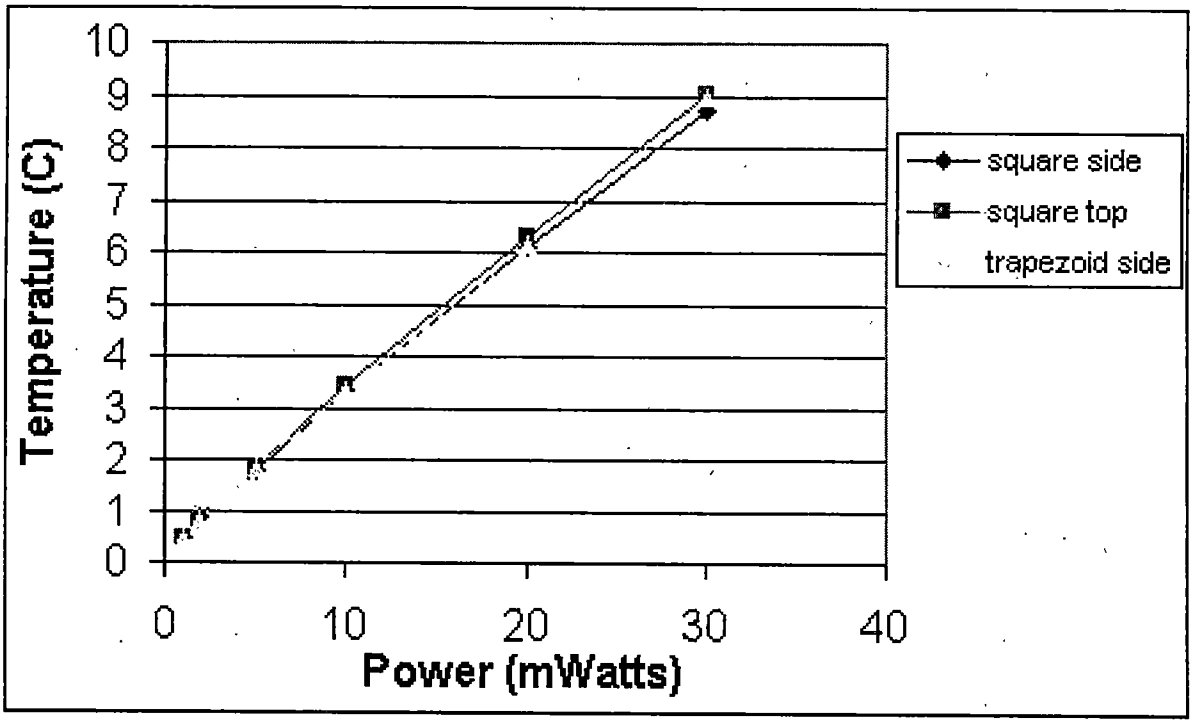

Figure 5.34: Maximum temperature plots for three ampule configurations.

Chapter 6

Conclusions and Recommendations

6.1 Conclusions

For the three ampule configurations it is evident that convection dominates the flow and temperature field. There is also a strong correlation between the vigor of the flow, based on maximum velocities, and the amount of heat input as shown in figure 5.33. This also is true for the maximum temperature which is seen in figure 5.34. Based on the maximal data and from isotherm and vector velocity plots it can be concluded that the amount of heat input can strongly affect the shape and strength of the flow field.

As the magnitude of gravity decreases, the effect of the heat input does as well. It is evident from figures 5.12, 5.23, and 5.31 that the maximum velocity drops off rapidly as the gravity decreases. There is a corresponding increase in maximum temperature from the reduction of gravity as shown in 5.13, 5.24, and 5.32. Both these results are observed in previous work and are physically realistic [6, 9]. Since the gravity term is reduced, the body force terms has less influence on the flow. This changes the flow from convection dominated to a conduction dominated. In a conduction dominated flow the maximum temperatures should be linear and this is observed in figures 5.13, 5.24, and 5.32 [19]. It is also shown in these figures that as the Rayleigh number decreases the maximum temperatures are approaching a stationary point. This is also an implication that conduction is dominating the flow. Ultimately a conduction dominated flow with its lower velocities circulates heat through a much smaller region which leads to higher observed temperatures. Since this behavior is observed it can be concluded that the numerical models are showing the physical behavior of the flow reasonably well. The next step must be to compare these results with the experimental case to see how accurate they are.

6.2 Recommendations

This work assumes that the quartz walls of the container do not significantly affect the solution and for a first approximation this may be reasonable. This view is based on the lack of energy absorption by quartz when a UV laser is incident on it. This ignores the conduction that will occur between the warmer heated fluid and the cooler unheated wall. In regime of 1 g this is likely to be insignificant as the high velocity of the fluid will pass heat to a larger amount of the wall with only small temperature difference due to the dominance of convection. As the magnitude of the gravity decreases the velocity of the fluid will decrease and conduction will begin dominating the flow. This will cause the heat to flow to a small portion of the wall where temperatures will increase. Ultimately when the steady state is reached the lower gravity case should have a slightly higher overall velocity than would the case where no wall conduction was assumed. When this problem is addressed in the non-dimensional sense it is in the lower Rayleigh numbers that the flow is dominated by conduction.

This leads to the recommendation that the lower g, or Rayleigh number, cases be run with the addition of a finite thickness quartz wall. This modeling can be done with FIDAP since it has conduction heat transfer and solid material capabilities. With this addition there may be some improvement in the lower velocity regimes.

It will also be extremely critical to find more useful estimators of characteristic temperatures and velocities. For this thesis the maximum temperature and maximum velocity were compared to the amount of heat flux. There is some question as to how well these quantities are as predictors of the vigor of the flow field. When the Rayleigh number is compared to the maximum velocity, Reynolds number, and Froude number some inconsistencies are observed between the side heating rectangular ampule and the side heating trapezoidal ampule. This leads one to question as to how much effect does geometry have on maximum velocity. Because the maximum velocities occur slightly above the heater, the geometry should have very little effect. Thus it is necessary to find a quantity that gives a better estimate of the velocity field's overall strength. A quantity that incorporates some integrated value of the velocity field or the circulation of the flow field might provide more useful data.

The last recommendation is to reconsider this problem non-dimensionally. By doing this it would provide a clearer picture of the physics of the flow by reducing a great number of variables down to a single parameter. Rather than describe flows in terms of the gravity vector, heat flux input, physical properties, and geometry considerations one would only need to consider the important non-dimensional parameters such as Rayleigh number and Prandtl number. The increased generality of the data would improve its usefulness to future work by allowing easier comparisons.

Bibliography

[1] Service, Robert A. "Nonlinear Competition Heats Up." *Science* 31 Mar. 1995: 1918-1921

[2] Gamire, Elsa "Nonlinear Optics." *Physics Today* May 1994: 23-24

[3] Islam, Mohammed N. "Ultrafast Switching With Nonlinear Optics." *Physics Today* May 1994: 34-40.

[4] Hellmans, Alexander "Chaos Keeps Data Under Wraps." *Science* 2 May 1997: 679.

[5] Marder, Seth R. and Perry, Joseph W. "Nonlinear Optical Polymers: Discovery to Market in 10 Years?" *Science* 25 Mar. 1994: 1706-1707.

[6] Frazier, D.O., R.J. Hung, M.S. Paley, and Y.T. Long. "Effects of Convection During the Photodeposition of Polydiacetylene Thin Films." *Journal of Crystal Growth* 173 (1997): 172-181.

[7] Antar, Basil N. and Vappu S. Nuotio-Antar. *Fundamentals of Low Gravity Fluid Dynmaics and Heat Transfer* Boca Raton, FL.: CRC Press, 1993.

[8] Kleinstreuer, Clement *Engineering Fluid Dynamics* Cambridge, UK: Cambridge Press, 1997.

[9] Gossian, Gregory James. "Numerical Modeling of a 3-D Buoyancy Driven Convective Flow" Diss. University of Tennessee, 1997.

[10] Reddy, J.N. *An Introduction to the Finite Element Method 2nd. Edition* New York: McGraw-Hill, 1993.

[11] Chung, T.J. *Finite Element Analysis in Fluid Dynamics* New York:McGraw-Hill, 1978.

[12] Chapra, Steven C. and Raymond P. Canale. *Numerical Methods for Engineers 2nd. Edition* New York: McGraw-Hill, 1988.

[13] Fluid Dynamics International, Inc. *FIDAP 7.0 Examples.* Evanston, IL.: Fluid Dynamics International, 1993.

[14] Upson C.D., P.M. Gresho, R.L. Lee.*Finite Element Simulations of Thermally Induced Convection in an Enclosed Cavity* Livermore, CA:Lawrence Livermore Laboratory, 1980.

[15] Kimura, S. and A. Bejan. "The Boundary Layer Natural Convection Regime in a Rectangular Cavity with Uniform Heat Flux from the Side." *Journal of Heat Transfer* 106 (1984): 98-103.

[16] Malhotra, R., W.E. Proce, L.A. Woolf, and A.J. Easteal. "Thermodynamic Properties of 1,2-Dichloroethane" *International Journal of Thermophyics* 11.5 (1990): 835-861.

[17] Yaws, Carl L. and Xiang Pan "Liquid Heat Capacity for Organics" *Chemical Engineering* Apr. 1992: 130-135.

[18] Qun-Fang, Lei. Lin Rui-Sen, Ni Dan-Yun, and Hou Yu-Chun. "Thermal Conductivities of Some Organic Solvents and Their Binary Mixtures" '*Journal of Chemical and Engineering Data* 42.5 (1997): 971-974

[19] Kakac, Sadik S. and Yaman Yener. *Heat Conduction 3rd. Edition* Washington, DC:Taylor & Francis, 1993.

[20] Bejan Adrian *Convection Heat Transfer 2nd. Edition* New York: Wiley, 1995.

Appendix

Appendix A

FIPOST Source Code for Extracting Data for Tecplot File Conversion

```
device(nographics)
fipost()
neutral(x,file="x.neut")
neutral(y,file="y.neut")
neutral(z,file="z.neut")
neutral(ux,file="ux.neut")
neutral(uy,file="uy.neut")
neutral(uz,file="uz.neut")
neutral(temp,file="temp.neut")
end
end
```

Appendix B

FORTRAN Source Code for Building a Tecplot File

```
      program main

      integer i, j, node, nmax
      real null, x, y, z, ux ,uy, uz, temp
      character*100 store, nodes

      open(1, file='x.FDNEUT')
      open(2, file='y.FDNEUT')
      open(3, file='z.FDNEUT')
      open(4, file='ux.FDNEUT')
      open(5, file='uy.FDNEUT')
      open(6, file='uz.FDNEUT')
      open(7, file='temp.FDNEUT')
      open(8, file='fidap.data')

100   format(f9.6,1x,f9.6,1x,f9.6,1x,f15.11,f15.11,f15.11,f15.11)
110   format(i5,1x,f12.9,1x,f12.9,1x,f12.9)
      do 200 i = 1, 11985
        read(1,*) store
        if (store .eq. 'NO.') then
          read(1,*) nodes*
          write(8,115) nodes
        endif
        if (store .eq. 'NODAL') then
          write(8,100) store
          read(1,*) node , x, y, z
          write(8,110) node,  x, y, z
```

```
         end if
c       reads first line of neutral file into null variable
        do 200 i = 1, nodes
           read(1,*) null,x,null,null,null
           read(2,*) null,y,null,null,null
           read(3,*) null,z,null,null,null
           read(4,*) null,ux,null,null,null
           read(5,*) null,uy,null,null,null
           read(6,*) null,uz,null,null,null
           read(7,*) null,temp,null,null,null
           write(8,100) x, y, z, ux, uy, uz, temp
200     continue
        stop
        end
```

Appendix C

Square Ampule With Side Heater FIMESH Input File

```
Title
10mWatt Side Heater with Dichloroethane
FIMESH(3-D,IMAX=7,JMAX=7,KMAX=5)
$mwatt=10
$flux=1.216E-3
$density=1.2436
$sheat=0.2093
$beta=1.2E-3
$viscosity=8.15E-3
$conductivity=3.208E-4
$g=981
$ct = 2.6
$cb = 1.78
$w = 0.5
$ro = 0.1768
EXPI
1 0 7 0 11 0 17
EXPJ
1 0 9 0 13 0 47
EXPK
1 0 7 0 15
POINT
/# I  J  K      X      Y      Z
10  3  3  1   -$ro  -$ro
11  5  3  1    $ro  -$ro
12  5  5  1    $ro   $ro
13  3  5  1   -$ro   $ro
```

```
20  1  3  1   -$w   -$ro
21  7  3  1    $w   -$ro
22  1  5  1   -$w    $ro
23  7  5  1    $w    $ro
30  1  1  1   -$w   -$cb
31  3  1  1   -$ro  -$cb
32  5  1  1    $ro  -$cb
33  7  1  1    $w   -$cb
40  1  7  1   -$w    $ct
41  3  7  1   -$ro   $ct
42  5  7  1    $ro   $ct
43  7  7  1    $w    $ct
50  0  0  0    0      0
130 1  1  3   -$w   -$cb    $w
230 1  1  5   -$w   -$cb     1

Refpoint
110  3  3  3
111  5  3  3
112  5  5  3
113  3  5  3
120  1  3  3
121  7  3  3
122  1  5  3
123  7  5  3
131  3  1  3
132  5  1  3
133  7  1  3
140  1  7  3
141  3  7  3
142  5  7  3
143  7  7  3

210  3  3  5
211  5  3  5
212  5  5  5
213  3  5  5
220  1  3  5
221  7  3  5
222  1  5  5
223  7  5  5
231  3  1  5
```

```
232  5  1  5
233  7  1  5
240  1  7  5
241  3  7  5
242  5  7  5
243  7  7  5

Line
30 130 5 3
230 130 5 3
20 22
23 21

20 30 5 3
21 33 5 3
30 31 5 3
33 32 5 3
31 32
10 31 5 3
11 32 5 3

40 22 5 3
41 13 5 3
42 12 5 3
43 23 5 3
40 41 5 3
43 42 5 3
41 42

Arc
10 11 50
11 12 50
12 13 50
13 10 50

Surface
30 43

Cdrive
43 30 30 130
143 130 130 230
```

```
ELEMENTS(BRICK,NODES=8,ENTITY="fluid")
30 243
ELEMENTS(BOUNDARY,FACE,ENTITY="coldwall")
30 21
20 13
11 23
22 43
30 240
230 243
233 43
240 43
230 33
ELEMENTS(BOUNDARY,FACE,ENTITY="hotwall")
10 12
END
FIPREP
PROBLEM(3-D,NONLINEAR,BUOYANCY)
PRESSURE(PENALTY=1.E-8,DISCONTINUOUS)
SPECIFICHEAT(CONSTANT=$sheat)
VISCOSITY(CONSTANT=$viscosity)
VOLUMEX(CONSTANT=$beta)
GRAVITY(MAGNITUDE=$g,THETA=-90,PHI=90)
CONDUCTIVITY(CONSTANT=$conductivity)
EXECUTION(RESTART)
SOLUTION(N.R.=7,VELCONV=.001,RESCONV=.001)
DENSITY(CONSTANT=$density)
DATAPRINT(NORMAL,PAGE,NODES)
POSTPROCESS
ENTITY(FLUID,NAME="fluid")
ENTITY(PLOT,NAME="coldwall")
ENTITY(PLOT,NAME="hotwall")
RENUMBER(PROFILE)
BCNODE(VELOCITY,ZERO,ENTITY="coldwall")
BCNODE(VELOCITY,ZERO,ENTITY="hotwall")
BCNODE(TEMPERATURE,ZERO,ENTITY="coldwall")
BCFLUX(HEAT,CONSTANT=$mwatt*$flux,ENTITY="hotwall")
RENUMBER(PROFILE)
END
CREATE(FISOLV
```

Appendix D

Square Ampule With Top Heater FIMESH Input File

```
Title
Top Heating 1x1x4.38cm 10mWatt Dichloroethane
FIMESH(3-D,IMAX=7,JMAX=7,KMAX=3)
$mwatt=10
$flux=1.216E-3
$density=1.2436
$sheat=0.2093
$beta=1.2E-3
$viscosity=8.15E-3
$conductivity=3.208E-4
$g=981
$w = 0.5
$ro = 0.1768
EXPI
1 0 7 0 11 0 17
EXPJ
1 0 7 0 11 0 17
EXPK
1 0 33
POINT
/# I  J  K      X      Y      Z
10  3  3  1   -$ro  -$ro
11  5  3  1    $ro  -$ro
12  5  5  1    $ro   $ro
13  3  5  1   -$ro   $ro
20  1  3  1   -$w   -$ro
21  7  3  1    $w   -$ro
```

```
22  1  5  1   -$w    $ro
23  7  5  1    $w    $ro
30  1  1  1   -$w   -$w
31  3  1  1   -$ro  -$w
32  5  1  1    $ro  -$w
33  7  1  1    $w   -$w
40  1  7  1   -$w    $w
41  3  7  1   -$ro   $w
42  5  7  1    $ro   $w
43  7  7  1    $w    $w
50  0  0  0    0      0
130 1  1  3   -$w   -$w   -4.38

Refpoint
110  3  3  3
111  5  3  3
112  5  5  3
113  3  5  3
120  1  3  3
121  7  3  3
122  1  5  3
123  7  5  3
131  3  1  3
132  5  1  3
133  7  1  3
140  1  7  3
141  3  7  3
142  5  7  3
143  7  7  3

Line
30 130 5 3
20 22
23 21

30 20 5 3
33 21 5 3
30 31 5 3
33 32 5 3
31 32
31 10 5 3
32 11 5 3
```

```
40 22 5 3
41 13 5 3
42 12 5 3
43 23 5 3
40 41 5 3
43 42 5 3
41 42

Arc
10 11 50
11 12 50
12 13 50
13 10 50

Surface
30 43

Cdrive
43 30 30 130

ELEMENTS(BRICK,NODES=8,ENTITY="fluid")
30 143
ELEMENTS(BOUNDARY,FACE,ENTITY="coldwall")
30 21
20 13
11 23
22 43
30 140
130 143
133 43
140 43
130 33
ELEMENTS(BOUNDARY,FACE,ENTITY="hotwall")
10 12
END
FIPREP
PROBLEM(3-D,NONLINEAR,BUOYANCY)
PRESSURE(PENALTY=1.E-8,DISCONTINUOUS)
SPECIFICHEAT(CONSTANT=$sheat)
VISCOSITY(CONSTANT=$viscosity)
VOLUMEX(CONSTANT=$beta)
```

```
GRAVITY(MAGNITUDE=$g,THETA=0,PHI=0)
CONDUCTIVITY(CONSTANT=$conductivity)
EXECUTION(RESTART)
SOLUTION(N.R.=7,VELCONV=.001,RESCONV=.001)
DENSITY(CONSTANT=$density)
DATAPRINT(NORMAL,PAGE,NODES)
POSTPROCESS
ENTITY(FLUID,NAME="fluid")
ENTITY(PLOT,NAME="coldwall")
ENTITY(PLOT,NAME="hotwall")
RENUMBER(PROFILE)
BCNODE(VELOCITY,ZERO,ENTITY="coldwall")
BCNODE(VELOCITY,ZERO,ENTITY="hotwall")
BCNODE(TEMPERATURE,ZERO,ENTITY="coldwall")
BCFLUX(HEAT,CONSTANT=$mwatt*$flux,ENTITY="hotwall")
RENUMBER(PROFILE)
END
CREATE(FISOLV)
```

Appendix E

Trapezoidal Ampule with Side Heater FIMESH Input File

```
Title
10mWatt, Trapezoidal Geometry w/ 0.5cm heater, dichloroethane
FIMESH(3-D,IMAX=7,JMAX=7,KMAX=7)
$power=10
$flux=1.216E-3
$density=1.2436
$sheat=0.2093
$beta=1.2E-3
$viscosity=8.15E-3
$conductivity=3.208E-4
$g=981
$l = 1.64
$wa = 1.525
$wb = 0.55
$ro = 0.1768
$cl = 2.0
EXPI
1 0 9 0 13 0 21
EXPJ
1 0 7 0 11 0 29
EXPK
1 0 0 0 0 0 15
POINT
/# I  J  K      X     Y     Z
1  1  1  1    -$wa   -$l    0
2  3  1  1    -$ro   -$l    0
```

```
3  5  1  1     $ro   -$l    0
4  7  1  1     $wa   -$l    0
5  1  3  1    -$wa   -$ro   0
6  3  3  1    -$ro   -$ro   0
7  5  3  1     $ro   -$ro   0
8  7  3  1     $wa   -$ro   0
9  1  5  1    -$wa    $ro   0
10  3  5  1   -$ro    $ro   0
11  5  5  1    $ro    $ro   0
12  7  5  1    $wa    $ro   0
13 1  7  1    -$wa    $l    0
14 3  7  1    -$ro    $l    0
15 5  7  1     $ro    $l    0
16 7  7  1     $wa    $l    0
50 0  0  0     0      0     0

101  1  1  7    -$wb   -$l    $cl
102  3  1  7    -$ro   -$l    $cl
103  5  1  7     $ro   -$l    $cl
104  7  1  7     $wb   -$l    $cl
105  1  3  7    -$wb   -$ro   $cl
106  3  3  7    -$ro   -$ro   $cl
107  5  3  7     $ro   -$ro   $cl
108  7  3  7     $wb   -$ro   $cl
109  1  5  7    -$wb    $ro   $cl
110  3  5  7    -$ro    $ro   $cl
111  5  5  7     $ro    $ro   $cl
112  7  5  7     $wb    $ro   $cl
113  1  7  7    -$wb    $l    $cl
114  3  7  7    -$ro    $l    $cl
115  5  7  7     $ro    $l    $cl
116  7  7  7     $wb    $l    $cl

Line
1 2 5 3
5 6 5 3
9 10 5 3
13 14 5 3
4 3 5 3
8 7 5 3
12 11 5 3
16 15 5 3
```

```
13 9 5 3
14 10 5 3
15 11 5 3
16 12 5 3
1 5 5 4
2 6 5 4
3 7 5 4
4 8 5 4

2 3
14 15
5 9
8 12

1 101 5 3 5 0.5
2 102 5 3 5 0.5
3 103 5 3 5 0.5
4 104 5 3 5 0.5
5 105 5 3 5 0.5
6 106 5 3 5 0.5
8 108 5 3 5 0.5
9 109 5 3 5 0.5
12 112 5 3 5 0.5
13 113 5 3 5 0.5
14 114 5 3 5 0.5
15 115 5 3 5 0.5
16 116 5 3 5 0.5


101 102 5 3
105 106 5 3
109 110 5 3
113 114 5 3
104 103 5 3
108 107 5 3
112 111 5 3
116 115 5 3
113 109 5 3
114 110 5 3
115 111 5 3
116 112 5 3
101 105 5 4
```

```
102 106 5 4
103 107 5 4
104 108 5 4

102 103
/106 107
/110 111
114 115
105 109
/106 110
/107 111
108 112

arc
6 7 50
7 11 50
11 10 50
10 6 50

Surface
1 8
5 10
6 11
7 12
9 16

cdrive
6 11 6 106
surface
101 108
105 110
107 112
109 116
1 113
1 104
4 116
13 116

3-D
1 116

ELEMENTS(BRICK,NODES=8,ENTITY="fluid")
```

```
1 116

ELEMENTS(BOUNDARY,FACE,ENTITY="coldwall")
1 8
5 10
7 12
9 16
101 116
1 113
1 104
4 116
13 116

ELEMENTS(BOUNDARY,FACE,ENTITY="hotwall")
6 11


END
FIPREP
PROBLEM(3-D,NONLINEAR,BUOYANCY)
PRESSURE(PENALTY=1.E-8,DISCONTINUOUS)
SPECIFICHEAT(CONSTANT=$sheat)
VISCOSITY(CONSTANT=$viscosity)
VOLUMEX(CONSTANT=$beta)
GRAVITY(MAGNITUDE=$g,THETA=-90,PHI=90)
CONDUCTIVITY(CONSTANT=$conductivity)
EXECUTION(RESTART)
SOLUTION(N.R.=10,VELCONV=.001,RESCONV=.001)
DENSITY(CONSTANT=$density)
DATAPRINT(NORMAL,PAGE,NODES)
POSTPROCESS
ENTITY(FLUID,NAME="fluid")
ENTITY(PLOT,NAME="coldwall")
ENTITY(PLOT,NAME="hotwall")
RENUMBER(PROFILE)
BCNODE(VELOCITY,ZERO,ENTITY="coldwall")
BCNODE(VELOCITY,ZERO,ENTITY="hotwall")
BCNODE(TEMPERATURE,ZERO,ENTITY="coldwall")
BCFLUX(HEAT,CONSTANT=$power*$flux,ENTITY="hotwall")
RENUMBER(PROFILE)
END
CREATE(FISOLV)
```

Vita

Thomas Holecek was born in Duluth, MN on December 19th, 1967. He graduated high school in 1986 from Harrison-Chilhowee Baptist Academy in Seymour, TN. After working for several years he attended and graduated from FonDuLac Community College with a A.A. degree. He then graduated with honors from the University of Wisconsin-Superior in 1997 with a B.S. in Mathematics and a minor in Physics. While at UW-Superior he co-authored a paper with Dr. Chad Scott and Sumedha Perera entitled *Improved Estimates for the Exterior Product's Submultiplication Constant* which was presented at the 1997 Syracuse University Graduate Mathematics Conference. He enrolled at UTSI in the summer of 1997 in the Masters of Engineering Science program studying under Dr. Basil Antar. During the course of his study he has been privileged to fly microgravity research flights onboard NASA's KC-135. Mr. Holecek served as Student Body Vice-President and AIAA Vice-President and has been active in both organizations since attending UTSI. He also helped manage many of the student organizations such as the boat and computer clubs. He has accepted a job with Lexmark International which he will be starting in April, 1999.